Control of PV-STATCOM: A Synchronverter Approach

MS (Research) Thesis

By

PANDYA YASH AVINASHBHAI

DISCIPLINE OF ELECTRICAL ENGINEERING

INDIAN INSTITUTE OF TECHNOLOGY INDORE

July,2021

Control of PV-STATCOM: A Synchronverter Approach

A THESIS

Submitted in fulfillment of the requirements for the award of the degree
of

Master of Science (Research)

by

PANDYA YASH AVINASHBHAI

DISCIPLINE OF ELECTRICAL ENGINEERING
INDIAN INSTITUTE OF TECHNOLOGY INDORE

July,2021

INDIAN INSTITUTE OF TECHNOLOGY INDORE

CANDIDATE'S DECLARATION

I hereby certify that the work which is being presented in the thesis entitled **Control of PV- STATCOM: A Synchronverter Approach** in the fulfillment of the requirements for the award of the degree of **MASTER OF SCIENCE (RESEARCH)** and submitted in the **DISCIPLINE OF ELECTRICAL ENGINEERING, Indian Institute of Technology Indore**, is an authentic record of my own work carried out during the time period from JULY,2019 to JULY,2021 under the supervision of Dr. Amod C Umarikar, Associate Professor, Discipline of Electrical Engineering, Indian Institute of Technology Indore, Indore, India.

The matter presented in this thesis has not been submitted by me for the award of any other degree of this or any other institute.

15/07/2021

Signature of the student with date
(PANDYA YASH AVINASHBHAI)

This is to certify that the above statement made by the candidate is correct to the best of my/our knowledge.

15/07/2021

Signature of the Supervisor of MS (Research) thesis (with date)
(DR. AMOD C UMARIKAR)

PANDYA YASH AVINASHBHAI has successfully given his MS (Research) Oral Examination held on Date: 8 September 2021

8/9/21

Signature of Chairperson (OEB) with date

8/9/2021

Signature(s) of Thesis Supervisor(s) with date

08/09/2021

Signature of Convener, DPGC with date

Saptarshi Ghosh 08/09/2021

Signature of Head of Discipline with date
HOD-EE (Officiating)

ACKNOWLEDGEMENTS

I would like to express my sincere and deepest gratitude for my supervisor Dr. Amod C Umarikar for his valuable and constructive guidance throughout this research work. I am also immensely thankful for the constant support and motivation which he has provided me.

I would also like to express my sincere gratitude to my thesis committee: Dr. Trapti Jain and Dr. Indrasen Singh for their encouragement and insightful comments which helped me a lot to widen my research perspectives.

I would also like to thank, my colleague and senior Mr. Ajinkya Sonawane for all his help and support during this research work of two years in MS(Research) program. Also, I would like to thank, my colleagues Mr. Dnyaneshwar Patale and Mr. Rahul Pawar for their valuable help in making this thesis a reality.

I would heartly like to thank my parents and my family members for their constant support, encouragement and belief in me during this journey.

PANDYA YASH AVINASHBHAI

Dedicated to my,

Lovely Parents

Abstract

As the use of renewable energy sources like solar PV and Wind Power in the power system is increasing and becoming dominant, the inertia of the power system is tending to reduce. The reason is that the renewable energy sources (wind and solar) have very less or no rotating mass with them like synchronous machine in conventional power generation. Due to that whenever there is a mismatch between power supply and demand, the variation in the system frequency will be faster and larger. Therefore, it is more difficult to keep the frequency in the normal range. It may result in cascade tripping and in the worst-case, blackouts. Inertia in the power system is important for the power system stability and it is one of the important factors in maintaining the power balance between supply and demand. Moreover, it slows down the rate of change of frequency during the disturbance. The increased penetration of the inverter based distributed generators (DGs) will diminish the power system inertia. To mitigate this challenge, a new concept called "virtual inertia" is becoming popular now-a-days. Based on this concept, inverter based DGs are supposed to emulate the synchronous generator rotor dynamics and supposed to provide virtual inertia support. This type of system is known as the "Virtual Synchronous Generator (VSG)". VSG have many different realizations and the "Synchronverter" is one of many realizations of VSG. This thesis is focused on the synchronverter application. Other than that, voltage regulation at the Point of Common Coupling (PCC) is also a challenging issue for the grid connected DG system. As the conventional voltage regulators like OLTC and shunt capacitors are not useful in the distribution system with DGs, STATCOM can be used for voltage regulation purpose. STATCOM which is called Static Synchronous Compensator can act as a synchronous condenser for the regulation of the PCC (Point of Common Coupling) voltage by injecting or absorbing appropriate amount of reactive power. Also, the inverter, based on solar energy, does not run on its full VA capacity throughout the day. After the active power generation if the inverter's remaining VA capacity can be utilized for the PCC voltage regulation, then the inverter VA capacity can be fully utilized and also it improves the grid integration of the DGs by providing good voltage regulation. With the above objectives, in this thesis, Synchronverter control and STATCOM (AC voltage control) both have been implemented as a single system for a grid-connected inverter with a photovoltaic source. In this thesis, all associated system components and its control design have been discussed. The performance of the proposed system is simulated using the Real Time Digital Simulator RTDS. It is observed that this approach of using a grid-connected inverter for multiple purposes (for Active and Reactive power control, providing the "Virtual Inertia" and PCC voltage

regulation), is really helpful for connecting more and more inverter-based renewable energy sources to the grid which may ensure better grid operations.

TABLE OF CONTENTS

LIST OF FIGURES

LIST OF TABLES

NOMENCLATURE

I_{sc}	Short circuit current of the PV cell
I_{pv}	Output current of the PV cell.
I_D	Diode current in equivalent circuit of the PV cell
V_{PV}	Output voltage of the PV cell
V_{oc}	Open circuit voltage of the PV cell
I_o	Diode saturation current in the equivalent circuit of the PV cell
T	Cell temperature
k	Boltzmann's constant
n_s	Number of series cells
n_p	Number of parallel cells.
V_{dc}	DC link voltage of the inverter
V_{LL}	Line to line RMS voltage at the AC side of the inverter.
$\omega(t)$	Time-varying angular frequency
$\theta(t)$	Time-varying phase angle
θ_0	Initial phase angle.
$\phi(t)$	Phase difference between *abc* reference frame and *d-q* reference frame
$\rho(t)$	Phase difference between rotating vector f(t) and the rotating *d-q* reference frame.
K_{pll}	PLL controller
G_f	Filter in PLL

V_{pcc-a}	A phase of PCC voltage
V_{pcc-b}	B phase of PCC voltage
V_{pcc-c}	C phase of PCC voltage
$\hat{V}$	Amplitude of the three phase PCC voltages
φ_{ref}	PLL angle
V_{pcc-d}	d component of PCC voltage space vector
V_{pcc-q}	q component of PCC voltage space vector
K_{pi}	Proportional gain of the PI compensator in current control loop
K_{ii}	Integral gain of the PI compensator in current control loop
K_{pv}	Proportional gain of the PI compensator in voltage control loop
K_{iv}	Integral gain of the PI compensator in voltage control loop
$V_{c_f}^{d}$	d component of the filter capacitor voltage space vector
$V_{c_f}^{q}$	q component of the filter capacitor voltage space vector
E^{d}	d component of the reference voltage in voltage control loop
E^{q}	q component of the reference voltage in voltage control loop
$V_{cf,ref}$	Reference voltage at the filter capacitor
V_{cf}	Actual voltage at the filter capacitor
C_f	Filter capacitor
PI_v	PI compensator of inner voltage control loop (VCL)
J_g	Inertia constant

T_m	Mechanical input torque,
T_e	Electromagnetic torque,
ω_g	Rotating speed of the synchronverter
ω_g^*	Reference value of the rotating speed of the synchronverter
D_p	Frequency droop coefficient
ΔT_m	Variation in input torque
$\Delta\omega_g$	Variation in the synchronverter angular speed
P_g^*	Reference input power
ω_N	Rated/nominal angular speed.
Ψ	Synchronverter excitation flux
θ_g	Virtual rotor angle (torque angle)
i_1^T	Inverter output current vector
V'_{pcc}	PCC voltage referred to the primary side of the isolation transformer
X'_2	Isolation transformer leakage reactance referred to the primary side of the transformer
J_g	Inertia constant
K	Control parameter for adjustment
D_q	Voltage droop coefficient
U_t	Line-to-line RMS voltage across the filter capacitor
U_t^*	Reference value of the U_t.
Q_g^*	Reference for the synchronverter output reactive power

Q_g	Synchronverter output reactive power
$G_p(s)$	Power Controller Dynamics
$G_q(s)$	Reactive Power Controller Dynamics
τ	Time constant of the filter
$H_{dc,uncomp}$	Uncompensated loop gain for DC link voltage control loop
P_{grid}	Active power injected into the grid
P_{Load}	Load active power
P_t	Active power injected into the PCC
Q_{grid}	Reactive power injected into the grid
Q_{Load}	Load reactive power
Q_t	Reactive power injected into the PCC
f_g	Synchronverter frequency
$i_{1,abc}$	Three phase Inverter output current
$i_{g,abc}$	Three phase Current injected into the grid
$i_{2,abc}$	Three phase Current injected into the PCC
$v_{pcc,abc}$	Three phase PCC voltage
$V_{pcc,ref}^{d}$	d component of the PCC voltage space vector
$V_{pcc,ref}^{q}$	q component of the PCC voltage space vector

ACRONYMS

PV	Photovoltaic
SG	Synchronous Generator
STATCOM	STATic synchronous COMpensator
PCC	Point of Common Coupling
AC	Alternating Current
DC	Direct Current
RRF	Rotating Reference Frame
SRF	Static Reference Frame
PLL	Phase Locked Loop
VSC	Voltage Source Converter
CSI	Current Source Inverter
VSI	Voltage Source Inverter
IGBT	Insulated Gate Bipolar Transistor
PWM	Pulse Width Modulation
SPWM	Sinusoidal Pulse Width Modulation
VSG	Virtual Synchronous Generator
CCL	Current Control Loop
VCL	Voltage Control Loop
APL	Active Power Loop

RPL	Reactive Power Loop
MPP	Maximum Power Point
MPPT	Maximum Power Point Tracking
RMS	Root Mean Square
PM	Phase Margin
GM	Gain Margin
RTDS	Real Time Digital Simulator
P&O	Perturb and Observe
GTDI	Giga Transceiver Digital Input
GTAO	Giga Transceiver Analog Output
GTAI	Giga Transceiver Analog Input
GTDO	Giga Transceiver Digital Output
HIL	Hardware in Loop
I/O	Input and Output
TOV	Temporary Overvoltage
OLTC	On-Load Tap changers
VA	Volt Ampere
VSCOM	Virtual Synchronous Compensator
VSM	Virtual Synchronous Machine

Chapter 1

Introduction

1.1 Background

Due to environmental, economic and technical reasons, the use of renewable energy sources for electricity generation is rapidly increasing. Mostly solar and wind energy systems are becoming more and more popular nowadays. Due to that the electrical power system is also moving from centralized generation to the distributed generation. As per the IEEE definition, Distributed Generation is “the generation of electricity by facilities that are sufficiently smaller than central generating plants to allow interconnection at nearly any point in a power system” [25]. The Photovoltaic system is one of the major renewable energy sources used for distributed generation.

In the past, Distributed Generators (DGs) were not required to regulate power generation according to the grid requirements. Previously as per the original grid codes like IEEE Standard 1547-2003, the DGs were required to produce as much energy as possible with a certain quality of the injected grid current during normal operation (which are the conventional current-controlled DGs) and should be disconnected from the grid under fault conditions. These standards were reasonable due to the low penetration of the renewable energy-based DGs into the grid. Due to a little amount of renewable energy share in the power system, large synchronous generators (SGs) can compensate any random power fluctuations in the power system due to their large amount of inertia and can maintain stability.

In present days, renewable energy share in the power system is increasing and renewable energy sources like PV and wind have very little inertia with them. In this case, more penetration of renewable energy sources in the power system is vulnerable for the whole power system stability. Hence these DGs are required to act as conventional SGs for the power system. The virtual Synchronous Generator (VSG) concept is based on this idea. The concept of VSG is to control the grid-connected inverter to emulate the behaviour of SG, which includes the droop characteristic and inertia support. According to the VSG concept, DG can control its active and reactive power according to the frequency and amplitude of the grid voltage respectively and its inertial characteristic can contribute to the total inertia of the grid.

1.2 Synchronverter

The synchronverter is a power electronic converter with a synchronous generator's mathematical model embedded into its controller so that it emulates the synchronous generator rotor dynamics and contributes inertia to the grid [13]. Synchronverter is basically a realization of the VSG (Virtual Synchronous Generator) concept [13],[14],[15],[17]-[21]. The whole idea behind the implementation of the synchronverter is to make VSC (Voltage Source Converter) behaves like a synchronous generator. Synchronverter emulates the swing equation (rotational inertia equation) and the excitation system of a Synchronous Generator (SG) and manages the supply of active and reactive power. Unlike SG, the inertia constants and droop constants of the synchronverter can be varied while it is operating. Synchronverter consists of the energy storage device like a battery or a supercapacitor, solid-state switches, filters and a control part which consists of active and reactive power loops.

In recent years, various improvements on synchronverter and VSG are suggested and implemented. The implementation of inner control loops, like voltage control loop (VCL) and current control loop (CCL), with a VSC, is important for the stability of voltage and current response [4]. Also, the voltage controller and current controller are an important part of the control system of an inverter-based microgrid [12]. In this thesis, inner control loops (VCL and CCL) are implemented with the synchronverter control.

1.3 Static Synchronous Compensator (STATCOM)

As grid integration of DGs is becoming more and more popular, it is important to mitigate the problems occurring due to the grid integration of the DGs. The challenges associated with the grid integration of the DGs are related to steady-state overvoltage, temporary overvoltage (TOV), voltage flicker and harmonics [22],[23]. Conventional devices like On-load tap changers (OLTC) and shunt capacitor banks are useful in conventional distribution systems where the power flow is unidirectional. But due to the integration of DGs, the power flow in the distribution system has become bidirectional and so the conventional voltage regulators are not operating satisfactorily [4],[33]. However, in a distribution system with DGs, the voltage regulation is possible by the use of STATic synchronous COMpensator (STATCOM) [24].

STATCOM is a shunt connected reactive power compensation device. It consists of a DC link capacitor, solid-state switches, filter elements and an interfacing transformer. STATCOM acts as a synchronous condenser for the regulation of the PCC (Point of Common Coupling) voltage by injecting or absorbing appropriate reactive power. It can provide reactive power as a capacitor and also can absorb the reactive power like an inductor. In this way, it can regulate the PCC voltage of a distribution system like a shunt capacitor or a shunt reactor. Practically, the solid-state switches used in the STATCOM are not lossless, hence STATCOM absorbs some amount of active power from the grid to compensate this loss. If it is equipped with an energy storage device or a source like a PV panel then it can also provide active power to the grid.

1.4 PV-STATCOM

As discussed in the previous chapter that STATCOM is a device that can exchange reactive power dynamically and acts as a reactive power compensator. Also, if it is equipped with any energy storage device then it can also provide active power. On the other hand, a conventional PV system also needs a VSC for DC to AC conversion and to deliver active power. As given in [4],[33], the combination of the conventional PV-system and the STATCOM is known as the PV-STATCOM and such system will have several advantages like: Full utilization of the inverter VA capacity, regulation of PCC voltage, cost-effective solution for increasing the connectivity of DGs in the distribution system.

Most of the time the conventional PV system runs below its rated power output because solar irradiance changes throughout the day and not available at night time. Due to that in the conventional PV system, the inverter is always underutilized. On the other hand, PV-STATCOM can use the remaining capacity of the inverter for voltage regulation by reactive power exchange [4].

When PV-STATCOM absorbs/injects reactive power by the remaining capacity of the inverter after the active power generation, then it is called “Partial STATCOM mode”. In this mode, the priority is injecting all active power generated by PV and then only reactive power exchange is done using the remaining capacity of the inverter.

When PV-STATCOM only absorbs/injects reactive power then it is called the “Full STATCOM mode”. In this mode, the PV panel is disconnected from the inverter system and active power generation is zero. Full

STATCOM mode is useful in night time or in the emergency conditions like faults or extremely under-voltage conditions when it is essential to maintain the PCC voltage on a certain level.

In this way, the PV-STATCOM system can fully regulate the PCC voltage with reactive power support.

1.5 PV-STATCOM with the synchronverter control

As described in section 1.2, due to the increased penetration of the renewable energy-based DG, it is essential to implement the virtual inertia concept in such DG system. Synchronverter is one of the popular VSG schemes which is used in this thesis. As described in section 1.3, PCC voltage regulation is also an important aspect of the grid-connected PV system. Therefore, the combination of the synchronverter and the PV-STATCOM can be a viable solution against the challenges like diminished inertia, intermittent nature of PV and poor voltage profile at PCC due to the grid integration of PV systems.

In this way, the "PV-STATCOM with synchronverter control system" can fully regulate the PCC voltage with reactive power support as well as it can provide inertia support and droop control. Hence, the "PV-STATCOM with synchronverter control system" can increase the connectivity of DGs in a distribution system.

Earlier, some work has been done on the implementation of VSG concept with STATCOM [29],[30],[31]. In [29], a controller is designed according to the mathematical model of synchronous generators that are operated in the compensator mode. In [30], a VSCOM (Virtual Synchronous Compensator) is proposed which adds virtual inertia in reactive power regulation of STATCOM. In [31], VSM (Virtual Synchronous Machine) concept is proposed as the alternative means to synchronize the grid-connected inverters, by developing a VSM based STATCOM controller operating as synchronous condenser. However, no studies have been done on a system which controls the active power as well as the reactive power, including virtual inertia, with STATCOM operation. In this thesis, synchronverter with inner voltage and current control loops has been implemented with the PV-STATCOM system.

1.6 Objective & scope of this thesis

The objective of this thesis is to design and implement the PV-STATCOM system with the synchronverter control strategy. Furthermore, as discussed in section 1.2, an improved synchronverter control, which is the “synchronverter with the inner current and voltage control loops” have been implemented in this thesis.

The scope of this thesis is:

- Development of a PV-STATCOM system with synchronverter consists of the inner control loops
- Validation of the model in real-time simulation for different conditions like “Full PV Mode”, “Partial STATCOM Mode” and “Full STATCOM Mode”.

1.7 Organization of the Thesis

This thesis comprises of total five chapters:

Chapter 1 discusses scope and objectives of the thesis along with the relevant available literature.

Chapter 2 discusses modeling of the whole system. It presents different components of the "PV-STATCOM with synchronverter control" system. Modeling of PV panel, MPPT, PV inverter, LCL filter, isolation transformer, PLL, inner control loops, synchronverter control, DC link voltage control and AC voltage regulator (STATCOM action) has been discussed.

Chapter 3 gives the details of control system design for the proposed system.

Chapter 4 consists of the real-time simulation results for the validation of the proposed system. Simulation is done for various loads and for various operating conditions like “Full PV Mode”, “Partial STATCOM Mode” and “Full STATCOM Mode”.

Chapter 5 concludes the thesis.

Chapter 2

Modeling of the PV-STATCOM with the synchronverter controller

2.1 Introduction

This chapter presents the modeling of the different components of the proposed system. Figure 2-1 shows schematic of the proposed system. Proposed system consists of the power part and the control part. Power part has a PV panel, three phase 2 level inverter, LCL filter, Active and Reactive power loads. Control part consists the Synchronverter-STATCOM control system. Synchronverter-STATCOM control consists of PLL (Phase Locked Loop), Inner Current control loop, Inner Voltage control loop, Synchronverter control, DC link voltage controller and PCC Voltage Regulator (AC Voltage control). The procedure for the design of these various system components is described in this chapter.

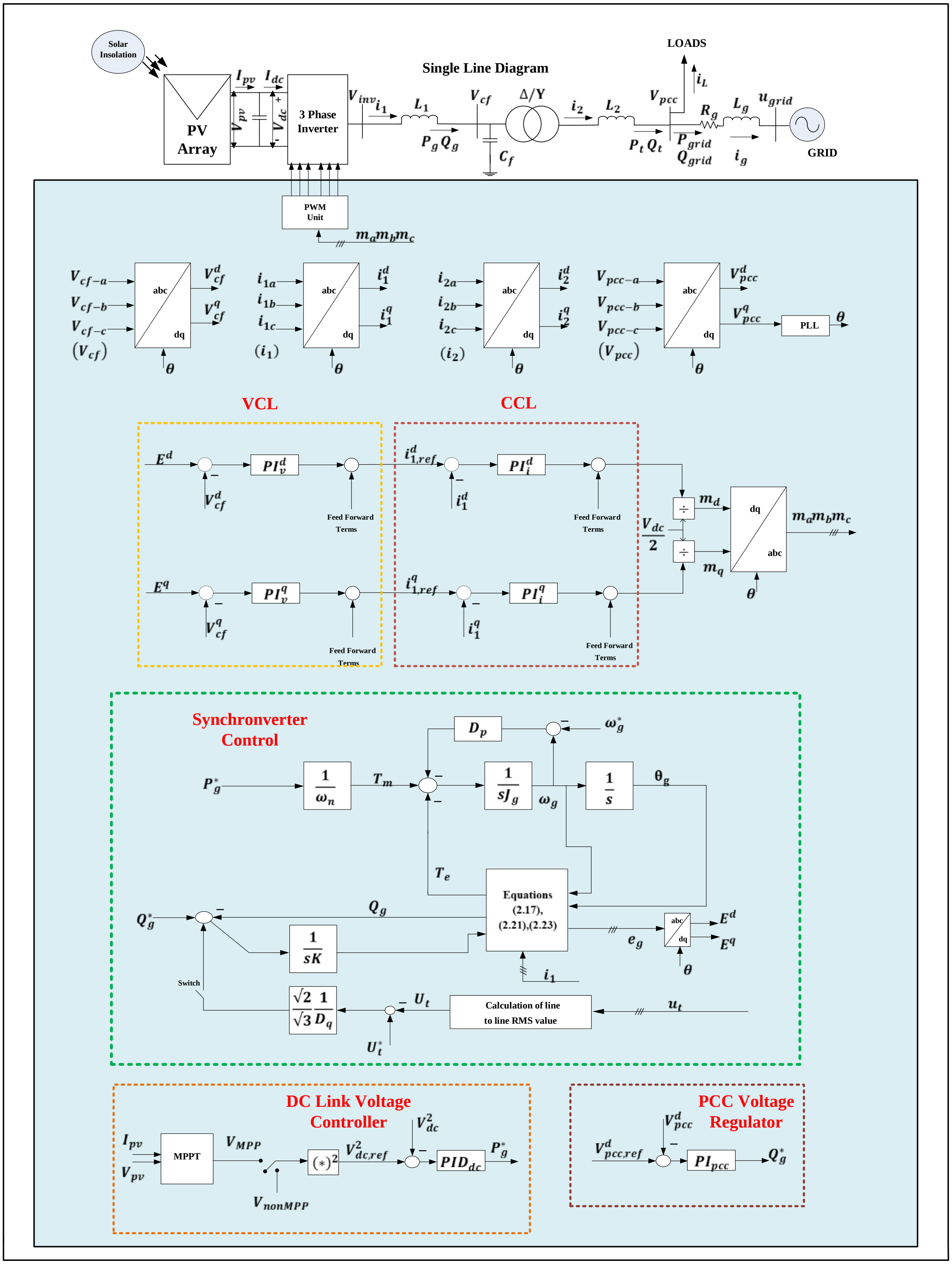

Figure 2-1: PV-STATCOM with synchronverter control

2.2 PV System Model

2.2.1 Photovoltaic Panel

Solar cell converts the solar energy into the electricity. As the Output power of a single cell is significantly low, many solar cells are connected in series-parallel combinations which is called module. In general, a solar panel consists of many arrays and each array have many modules [1]. Performance of the solar cell is mainly affected by the two factors: Solar radiation and temperature [2]. As shown in the below figure 2-1, current changes significantly with the irradiance, whereas the voltage changes significantly with temperature.

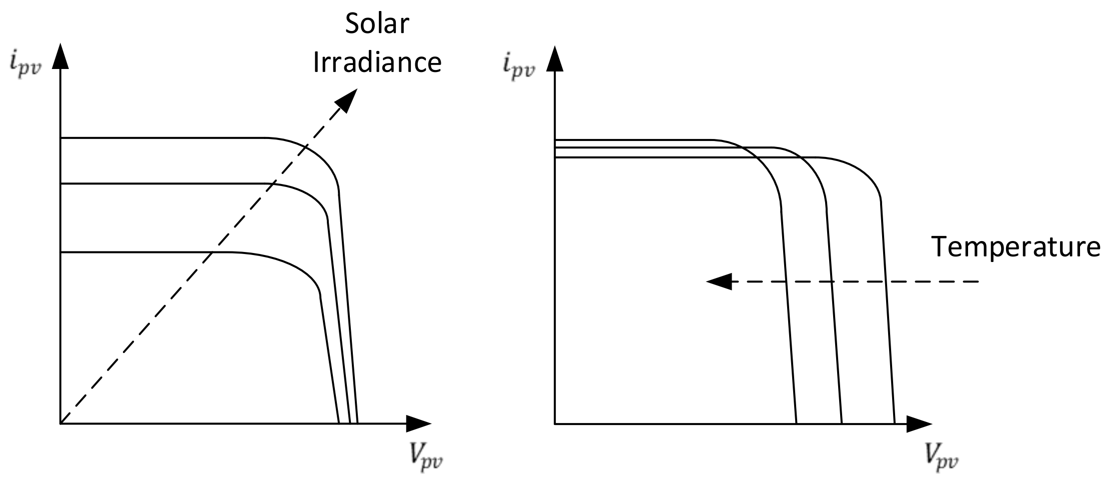

Figure 2-2: Solar cell *i-v* characteristic based on the variations of Irradiance and Temperature

As shown in the 2-2, solar cell gives maximum power at the particular voltage and current for the given condition of irradiance and temperature called Maximum Power Point (MPP). Figure 2-4 shows a simple equivalent circuit of a solar cell which has an ideal current source and a parallel diode.

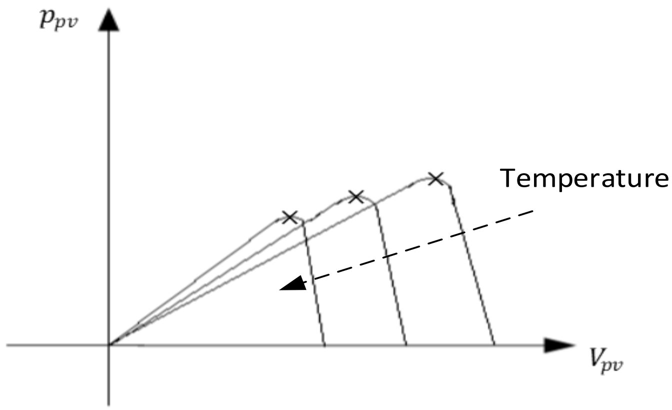

Figure 2-3: Power versus voltage characteristic of solar cell for different temperatures

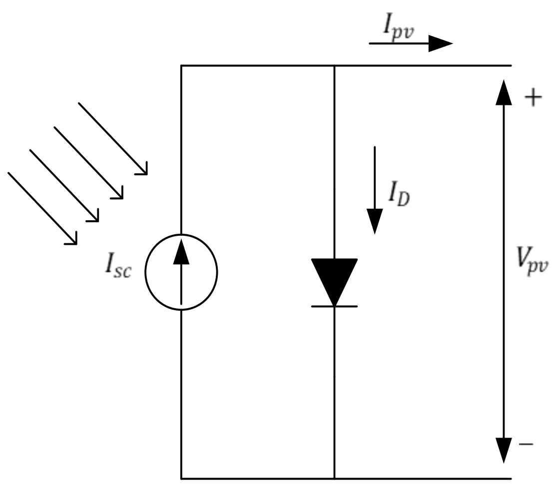

Figure 2-4: Solar cell equivalent circuit

I_{sc} is the short circuit current and I_{pv} is the output current of the PV cell. I_D is the diode current and V_{PV} is the output voltage of the PV cell.

$$I_{pv} = n_p(I_{sc} - I_D) = n_p I_{sc} - n_p I_o \left[e^{\left(\frac{qV_{pv}}{kTn_s}\right)} - 1 \right] \quad (2.1)$$

Where, I_o is the diode saturation current, electron charge q = $1.6e^{-19}$ coulomb, T is the cell temperature, k $=1.38e^{-23}$ is the Boltzmann's constant, n_s is the number of series cells and n_p is the number of parallel cells.

From equation (2.1), PV terminal voltage can be written as follows:

$$V_{pv} = \frac{kTn_s}{q} \ln\left(1 - \frac{I_{pv} - n_p I_{sc}}{n_p I_o}\right) \qquad (2.2)$$

2.2.2 Maximum Power Point Tracking (MPPT)

It is discussed in section 2.2.1, that the PV panel performs well in terms of power output, at low temperature and high solar irradiance. Also, according to PV characteristics shown in section 2.2.1, the PV panel provides maximum power output at a particular voltage and current and that point on the characteristic curve called Maximum Power Point (MPP). Various MPPT (Maximum Power Point Tracking) algorithms are used to achieve maximum output power from the solar panel at particular irradiance and temperature conditions. MPPT algorithms increase the efficiency of the solar panel. Mainly two MPPT algorithms are popular in grid connected PV system: Perturb & Observe (P&O) method and Incremental Conduction method [32].

For this thesis work, Perturb & Observe (P&O) method is used as the MPPT algorithm. P&O algorithm, perturbs the PV output voltage in one direction (increment or decrement) and then observes the corresponding change in the PV power output. If the change in power is positive (i.e., if power is increased), then the algorithm continues to move the voltage in the same direction; otherwise, it reverses the direction.

2.2.3 PV Inverter

PV Inverter is an important part of the PV system which is used to convert DC power into AC power. There are two types of PV inverters: CSI (Current Source Inverter) and VSI (Voltage Source Inverter). Three phase VSI (Voltage Source Inverter) is more popular in grid connected applications. Also, the different level VSI configurations are being used according to the applications. In this thesis Three Phase Two Level VSI is used. It consists of IGBT switches and a capacitor at the DC side known as DC link capacitor. The ripple current caused due to the switching of the IGBT switches have low impedance path through the DC link capacitor. In this thesis SPWM (Sinusoidal Pulse Width Modulation) technique is used as a switching technique for the PV inverter. The relation between the DC and the AC side voltage in the two level VSI configuration with SPWM technique is as follows:

$$\frac{\sqrt{2}}{\sqrt{3}}V_{LL} \leq \frac{V_{dc}}{2} \qquad (2.3)$$

Where, V_{dc} is the DC link voltage of the inverter and V_{LL} is the Line-to-Line RMS voltage at the AC side of the inverter.

2.2.4 LCL filter

Voltage Source Inverter (VSI) converts DC power into AC power. The power electronics switches of the VSI are switched using various PWM (Pulse Width Modulation) techniques. The Carrier wave and the reference wave are used in PWM techniques. The carrier wave frequency decides the switching frequency of the inverter switches. This switching frequency for VSI is generally chosen between 2 kHz and 15 kHz. Hence these switching frequencies reflect in the output current and voltage waveforms of the VSI. To attenuate these switching frequencies from the current to be injected by the VSI into the grid, VSI needs to be connected to the PCC through a filter. A series inductor is typically used as a filter, which highly depends on switching frequency and harmonic attenuation levels. A series inductor filter may have a higher voltage drop across it at the fundamental frequency and becomes bulky and inefficient [3]. Hence LCL filter is used generally for grid-connected applications of VSI. LCL filter is a third-order filter and provides better performance in removing the harmonics [4]. Figure 2-5 shows the LCL filter for the grid-connected application. In this thesis the LCL filter is designed according to [5].

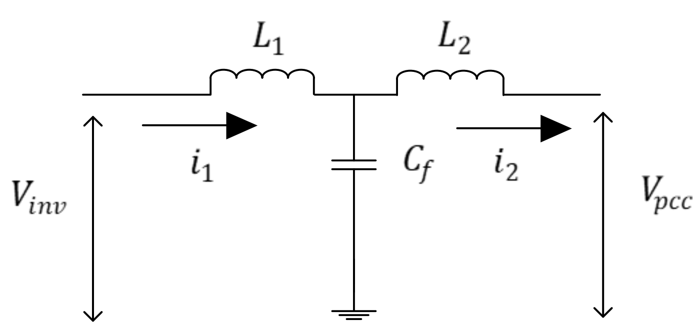

Figure 2-5: LCL filter for the grid connected converter

2.2.5 Isolation Transformer

An isolation transformer is used to provide galvanic isolation between the PV system and the utility system, also it is useful for providing voltage transformation. The most common configuration of transformer for the PV system isolation is Delta-Wye. In Delta-Wye configuration Delta winding is used on the PV side and grounded Wye is connected to the utility side [4].

2.3 Synchronverter-STATCOM control system

2.3.1 *abc* to *d-q* transformation

The *d-q* reference frame which is also known as rotating reference frame, transforms the sinusoidal signals into the equivalent DC signals. Figure 2-6 shows a vector $f(t)$ which rotates with time-varying frequency $\omega(t)$ in *abc* reference frame. $\theta(t)$ is the phase difference between the rotating vector $f(t)$ and the stationary axes in the *abc* reference frame. θ_0 is the initial phase angle. To achieve DC, the *d-q* reference frame needs to rotate with the same frequency $\omega(t)$. In Figure 2-6, $\varphi(t)$ is the phase difference between *abc* reference frame and *d-q* reference frame, whereas $\rho(t)$ is the phase difference between rotating vector $f(t)$ and the rotating *d-q* reference frame.

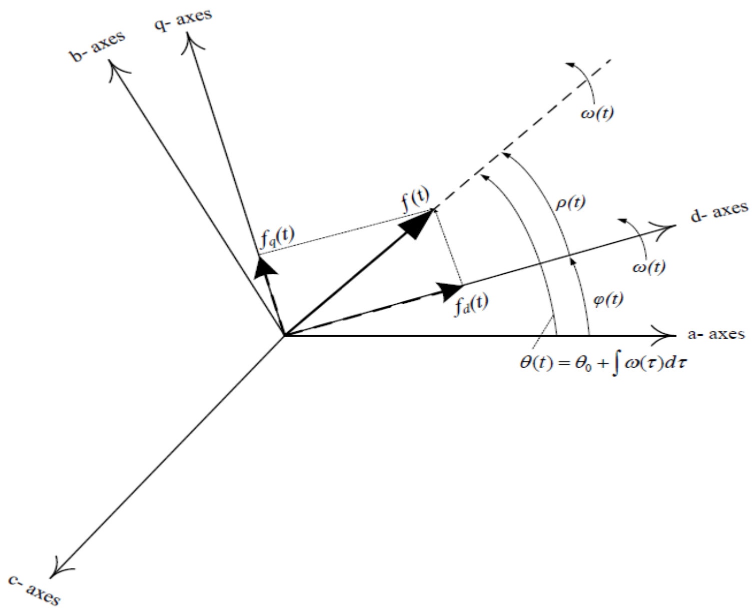

Figure 2-6: Phasor diagram of a parameter in *abc* and *d-q* frame

Below are the mathematical relations between *abc* and *d-q* reference frame used for the transformation between the two reference frames [6]. These transformations are used in the *d-q* to *abc* transformations for the proposed control system in this thesis, as shown in the figure 2-1.

$$\begin{bmatrix} f_d(t) \\ f_q(t) \end{bmatrix} = \frac{2}{3} C[\emptyset(t)] \begin{bmatrix} f_a(t) \\ f_b(t) \\ f_c(t) \end{bmatrix} \tag{2.4}$$

$$\begin{bmatrix} f_a(t) \\ f_b(t) \\ f_c(t) \end{bmatrix} = C[\emptyset(t)]^T \begin{bmatrix} f_d(t) \\ f_q(t) \end{bmatrix} \tag{2.5}$$

$$C[\emptyset(t)] = \begin{bmatrix} \cos[\emptyset(t)] & \cos[\emptyset(t) - \frac{2\pi}{3}] & \cos[\emptyset(t) + \frac{2\pi}{3}] \\ -\sin[\emptyset(t)] & -\sin[\emptyset(t) - \frac{2\pi}{3}] & \sin[\emptyset(t) + \frac{2\pi}{3}] \end{bmatrix} \tag{2.6}$$

$$C[\emptyset(t)]^T = \begin{bmatrix} \cos[\emptyset(t)] & -\sin[\emptyset(t)] \\ \cos[\emptyset(t) - \frac{2\pi}{3}] & -\sin[\emptyset(t) - \frac{2\pi}{3}] \\ \cos[\emptyset(t) + \frac{2\pi}{3}] & \sin[\emptyset(t) + \frac{2\pi}{3}] \end{bmatrix} \tag{2.7}$$

2.3.2 Phase Locked Loop (PLL)

In a grid-connected inverter system, it is important to synchronize the inverter system with the grid in terms of frequency and phase. Also as discussed in the previous section 2.3.1, $\varphi(t)$ must be equal to ωt for obtaining *d-q* transformation. Generally, a Phase Locked Loop (PLL) is used for obtaining phase and frequency to synchronize the reference current of an inverter with the grid voltage. In this thesis, PLL is used to extract the frequency and the phase angle of the PCC (Point of Common Coupling) voltage to synchronize the inverter system with the grid.

The below figure 2-7 shows the block diagram of PLL in the synchronous reference frame.

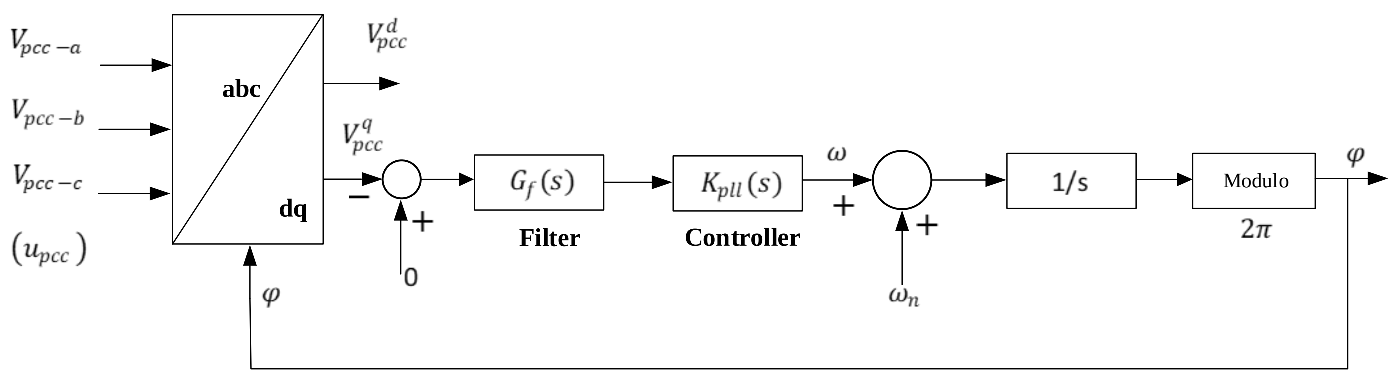

Figure 2-7: Phase Locked Loop (PLL) structure

As shown in the figure 2-7, three-phase PCC voltages are used as the input for the PLL and *d-q* components are obtained using the *abc* – *d-q* transformation. A filter block is used to extract the DC quantity of V_{pcc-q}. Phase is locked by making the q component zero, which is achieved by using a PI compensator. An integrator is used for getting the PCC voltage phase angle. The modulo divisor block is used to set the phase angle between 0 to 2π.

Considering, three phase PCC voltages as follows:

$$V_{pcc-a} = \hat{V}\cos(w_o t + \theta_o),\quad V_{pcc-b} = \hat{V}\cos\left(w_o t + \theta_o - \frac{2\pi}{3}\right),\quad V_{pcc-c} = \hat{V}\cos\left(w_o t + \theta_o + \frac{2\pi}{3}\right)$$

According to figure 2-6, $V_{pcc-q} = \hat{V}\sin(w_o t + \theta_o - \varphi)$

From the above figure 2-7, $\frac{d\varphi}{dt} = K_{pll} G_f \hat{V}\sin(w_o t + \theta_o - \varphi)$ (2.8)

Now φ is generally very near to $w_o t + \theta_o$, so, $\sin(w_o t + \theta_o - \varphi) \approx (w_o t + \theta_o - \varphi)$

Hence, (2.4) can be written as $\frac{d\varphi}{dt} = K_{pll} G_f \hat{V}(w_o t + \theta_o - \varphi)$ (2.9)

Also considering $(w_o t + \theta_o) = \varphi_{ref}$, then $\frac{d\varphi}{dt} = K_{pll} G_f \hat{V}(\varphi_{ref} - \varphi)$ (2.10)

According to (2.6) the control block diagram for the PLL design is as below.

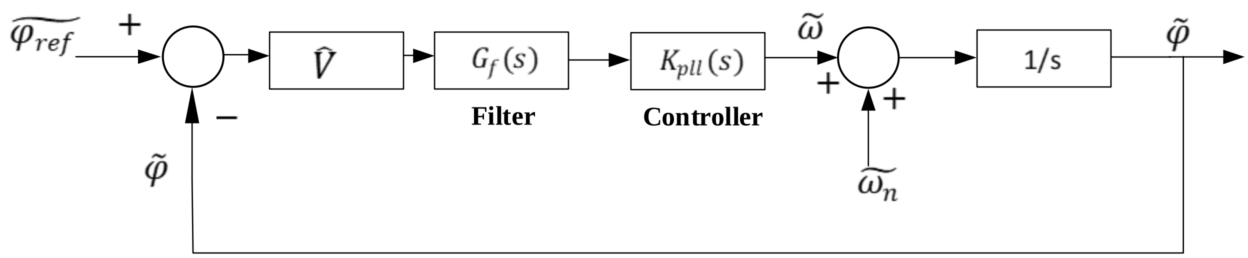

Figure 2-8: Control block diagram of the PLL

In the steady state, $\varphi_{ref} = \varphi$ and V_{pcc-q} becomes zero.

2.3.3 Inner Control loops

According to [9], the inner Voltage Control Loop (VCL) and the Current Control Loop (CCL) are important in the control of Voltage Source Converters (VSCs) for stable voltage and current response characteristics. In [10], the impacts of the inner control loops in Virtual Synchronous Generators (VSGs) have been investigated and concluded that the inner control loops are helpful to ensure transient stability [10]. Hence, the synchronverter control, implemented with the inner Voltage Control Loop (VCL) and the inner Current

Control Loop (CCL) is considered in this thesis. CCL is the inner most control loop and the VCL is the outer loop for the CCL.

2.3.3.1 Inner Current Control Loop

Design of the inner current control loop (CCL) is the same as the design of the conventional current control scheme for the Voltage Source Converters (VSC). The reference current signal for the CCL is available from the VCL. This reference signal is compared with the output current of the Inverter and the PI compensator is used for making current error to zero, ensuring the reference current is tracked by the output current of the inverter.

Block diagram for the current controller (CCL) is shown in the below figure 2-9. It consists of two PI compensators for *d* and *q* components i_1^d *and* i_1^q , with *d-q* decoupling and voltage feedforward terms in it.

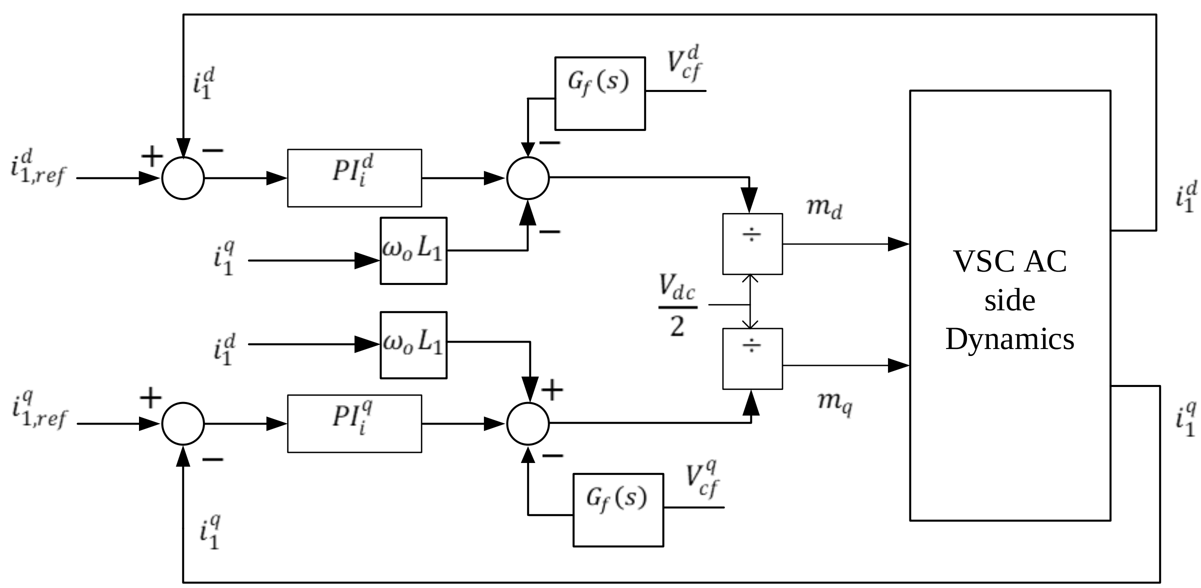

Figure 2-9: Structure of inner current control scheme in *d-q* reference frame

Here, $PI_i^d = PI_i^q = K_{pi} + \frac{K_{ii}}{s}$ (2.11)

K_{pi} and K_{ii} are the proportional and integral gain of the PI compensator respectively.

The Control system which is designed in the domain of SRF (Synchronous Rotating Reference Frame) consists of two same PI compensators each one for the *d* and *q* component of the inverter output current respectively. The control block diagrams for the CCL are shown below for both the *d* and *q* component of the current [6]. Here *d*-*q* decoupling terms and voltage feed-forward terms are neglected as they are considered as the disturbance signals for the system.

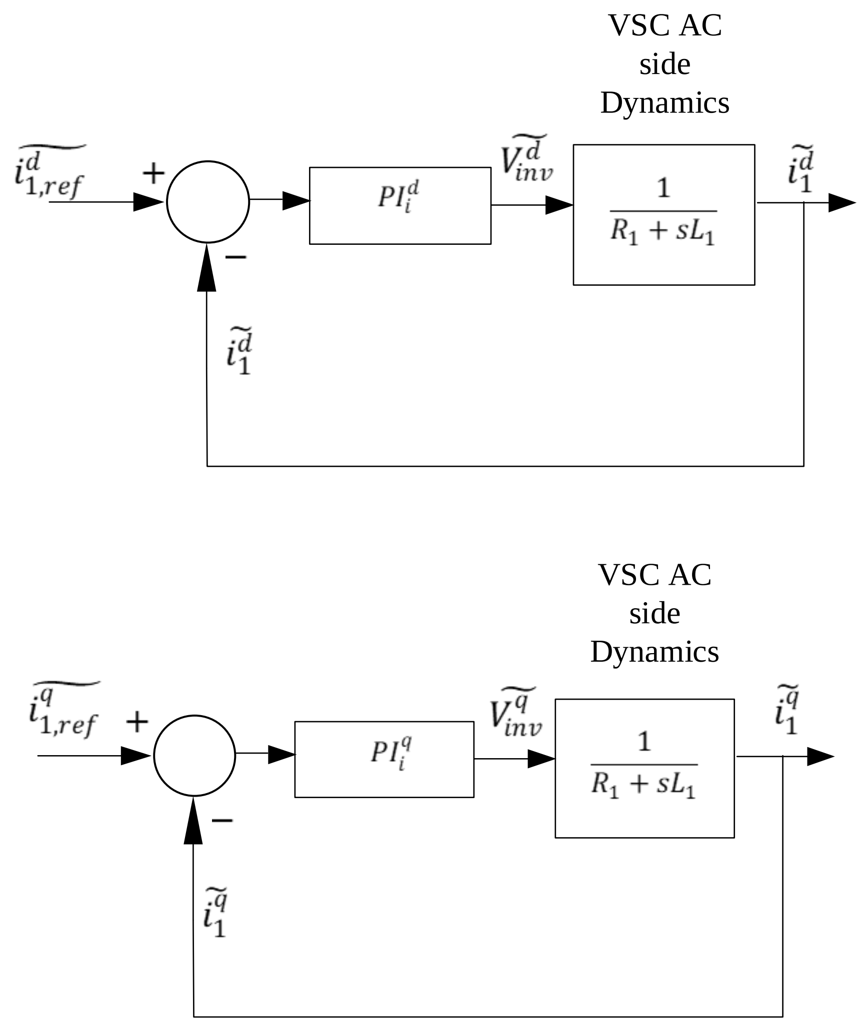

Figure 2-10: Control block diagram of the inner current control scheme

2.3.3.2 Inner Voltage Control Loop

The inner Voltage Control Loop (VCL) acts as the outer loop for the inner Current Control Loop (CCL). Therefore, the outputs of the VCL act as the reference signals for the CCL. As shown in the below figure 2-11, i_{1ref}^{d} and i_{1ref}^{q} are the output signals of the VCL which act as the input signals for the CCL. E^{d} and E^{q} are the reference input signals for VCL. The voltage reference signals E^{d} and E^{q} are provided by the synchronverter controller. As shown in the below figure 2-11, PI compensators with *d*-*q* decoupling terms and current feed-forward terms are used.

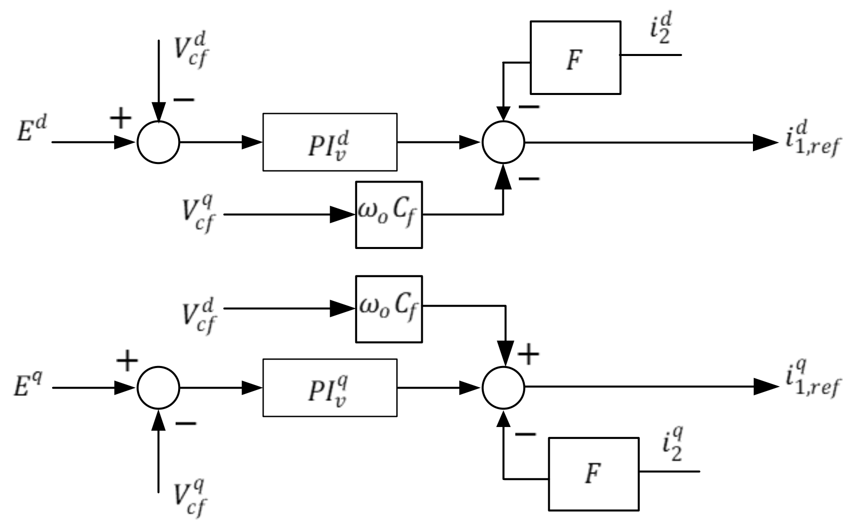

Figure 2-11: Structure of inner voltage control scheme in *d-q* reference frame

This voltage control loop settles the voltage across the filter capacitor $V_{c_f}^{d}$ and $V_{c_f}^{q}$ at the reference values of E^{d} and E^{q}.

Here, $PI_{v}^{d} = PI_{v}^{q} = K_{pv} + \frac{K_{iv}}{s}$ (2.12)

K_{pv} and K_{iv} are the proportional and integral gain of the PI compensator respectively.

Below is the control block diagram useful for the design of VCL. It also includes the LCL filter dynamics.

Here, $V_{cf,ref}$ and V_{cf} are the reference voltage and actual voltage at the filter capacitor C_f respectively.

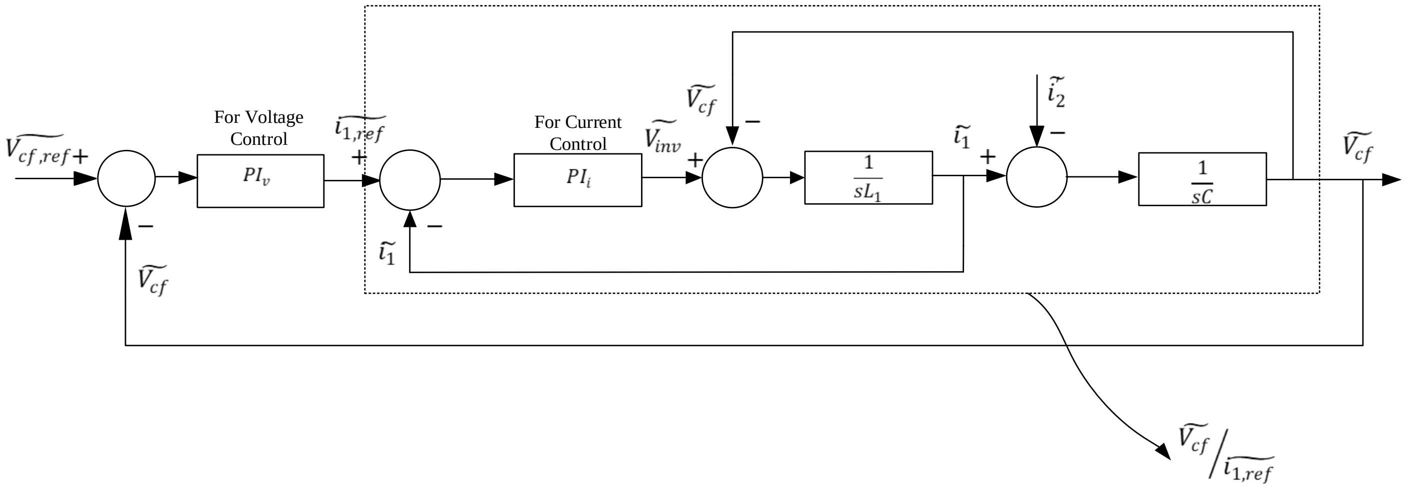

Figure 2-12: Control block diagram of the inner voltage control scheme

Using block shifting/reduction technique the above block diagram can be reduced to the below simplified reduced block diagram which is useful in designing PI_v for the VCL.

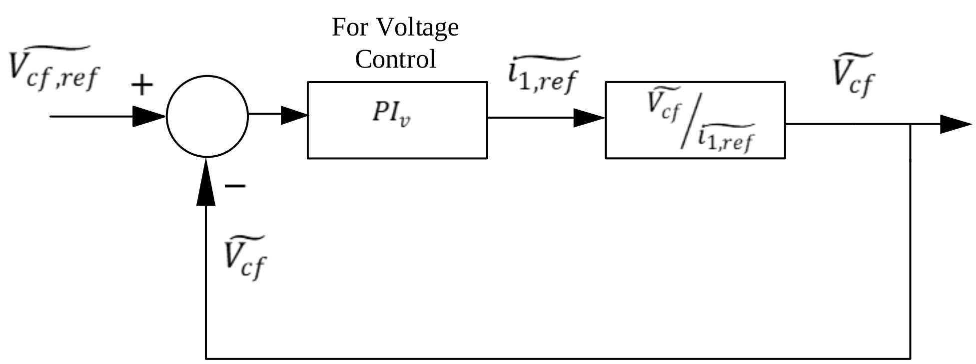

Figure 2-13: Simplified Control block diagram of the inner voltage control scheme

Here, $\frac{\widetilde{V_{cf}}}{\widetilde{i_{1,ref}}} = \frac{sK_{pi}+K_{ii}}{s^3L_1C_f + s^2C_fK_{pi} + s(1+C_fK_{ii})}$ (2.13)

2.3.4 Synchronverter

The synchronverter is a power electronic converter with a synchronous generator's mathematical model embedded into its controller, so that, it emulates synchronous generator rotor dynamics and contributes inertia to the grid [13]. Synchronverter controller consists of the Active Power Loop (APL) and the Reactive Power Loop (RPL). Both APL and RPL are described below:

2.3.4.1 Active Power Loop (APL) control

Active power Loop consists of the swing equation of the synchronous generator including the simplified governor droop action for frequency droop control.

$$J_g \frac{d\omega_g}{dt} = T_m - T_e - D_p\left(\omega_g - \omega_g^*\right) \qquad (2.14)$$

J_g is the inertia constant, T_m is the mechanical input torque, T_e is the electromagnetic torque, ω_g is the rotating speed of the synchronverter, ω_g^* is the nominal value of the ω_g and D_p is the frequency droop coefficient.

Where, $D_p = {}^{\Delta T_m}\!/_{\Delta\omega_g}$. (2.15)

ΔT_m is the amount of change in the input torque for $\Delta\omega_g$ variation in the angular speed. Also, the mechanical input torque $T_m = {}^{P_g^*}\!/_{\omega_N}$ (2.16)

P_g^* is the reference input power and ω_N is the rated angular speed.

In steady state, when $\omega_g = \omega_g^*$, P_g^* is a reference power for the synchronverter output power P_g and P_g becomes equal to P_g^* in steady state.

Also, P_g^* is decided by the DC link voltage controller which has been discussed in the later section 2.3.5. Now for the excitation flux Ψ which is obtained from the synchronverter RPL (Reactive Power Loop), the virtual rotor angle (torque angle) θ_g and the inverter output current i_1^T , the electromagnetic torque T_e can be expressed according to [14],

$$Te = \Psi i_1^T \left[\sin\theta_g \quad \sin(\theta_g - \frac{2\pi}{3}) \quad \sin(\theta_g + \frac{2\pi}{3}) \right]^T \tag{2.17}$$

$$\theta_g = \int_0^t \omega_g \, dt \tag{2.18}$$

Also, the Large Frequency Averaged Small Signal Model of the synchronverter control system can be considered as per [15]. The Large Frequency Averaged Small Signal Models for APL (Active Power Loop) and RPL (Reactive Power Loop) are shown in figure 2-14 and figure 2-15 respectively.

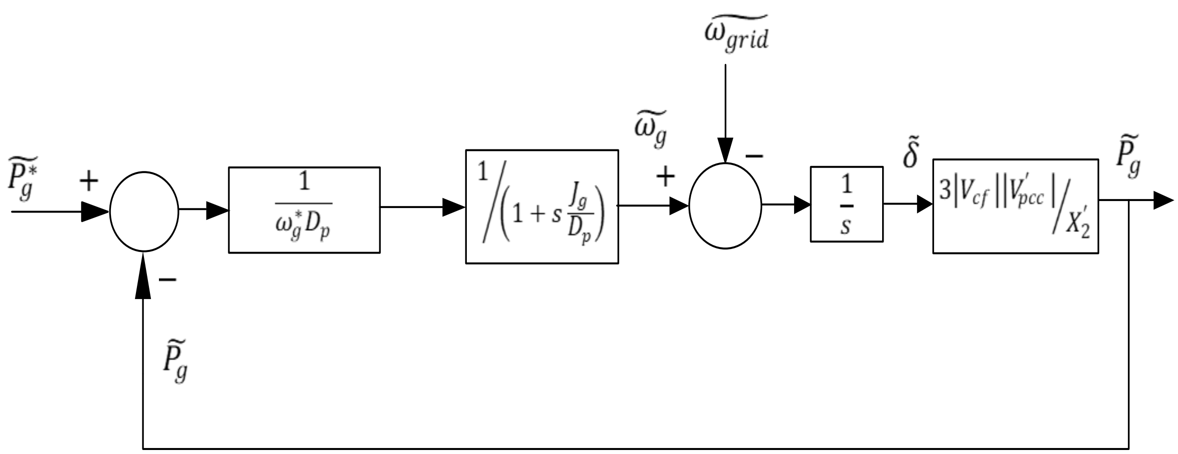

Figure 2-14: Small signal model of Active Power Loop (APL)

$|V_{cf}|$ and $|V'_{pcc}|$ are the RMS phase voltages at the Filter capacitor and at the Point of Common Coupling (PCC) respectively. Here V'_{pcc} and X'_2 are the referred quantities to the primary side of the transformer.

As per figure 2-14, according to $\frac{1}{1+s\frac{J_g}{D_p}}$, APL has time constant of $\tau_f = \frac{J_g}{D_p}$ which decides APL's speed of response and useful in deciding inertia constant J_g of the system.

$$J_g = D_p \tau_f \tag{2.19}$$

Here, the inner loops (CCL & VCL) control system dynamics can be omitted as the bandwidths of the synchronverter and the inner loops are well separated which is described in Chapter 3.

2.3.4.2 Reactive Power Loop (RPL) control

Reactive power Loop of the synchronverter regulates the reactive power of the synchronverter according to the voltage droop coefficient as shown below.

$$K\frac{d\Psi}{dt} = (Q_g^* - Q_g) + (\frac{\sqrt{2}}{\sqrt{3}})Dq(U_t^* - U_t) \tag{2.20}$$

where K is the control parameter for adjustment of RPL response speed, D_q is the voltage droop coefficient, U_t is the line-to-line RMS voltage across the filter capacitor and U_t^* is the reference value of the U_t.

Here, D_q = ${}^{\Delta Qg}/_{\Delta U_t}$, ΔQ_g is the amount of change in the input reactive power for ΔU_t difference in the synchronverter output voltage from U_t^*.

Also, Q_g^* is decided by the PCC voltage regulator which has been discussed in the later section 2.3.6.

When voltage droop is disabled, Q_g^* is a reference reactive power for the synchronverter output reactive power Q_g and in steady state Q_g becomes equal to Q_g^*.

Q_g is calculated as per the below expression according to [14],

$$Qg = -\omega_g \Psi i_1^T \left[\cos\theta_g \quad cos(\theta_g - \frac{2\pi}{3}) \quad cos(\theta_g + \frac{2\pi}{3})\right]^T \tag{2.21}$$

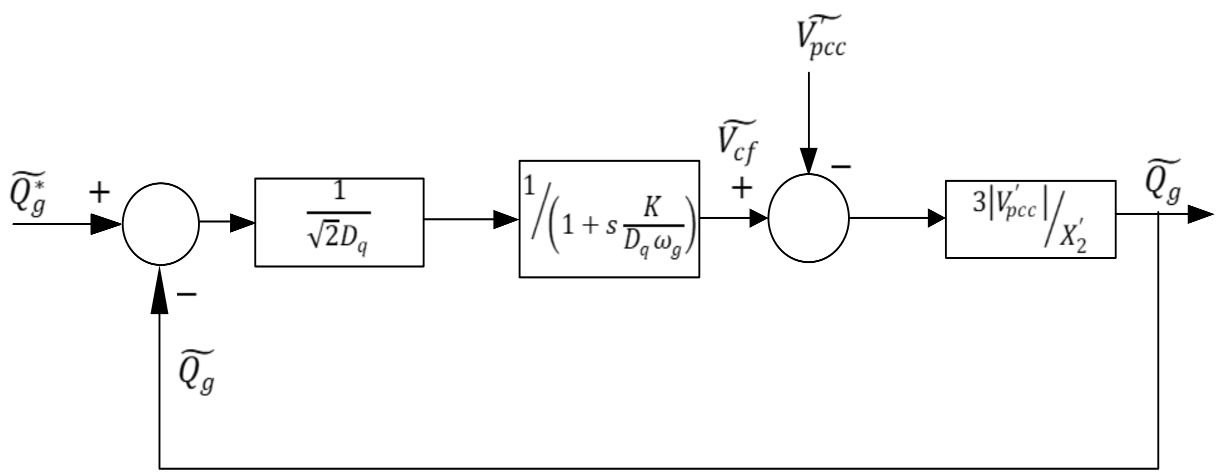

Figure 2-15: Small signal model of Reactive Power Loop (RPL)

As per figure 2-15, according to $\frac{1}{1+s\frac{K}{D_q\omega_g}}$, RPL has the time constant of $\tau_v = \frac{K}{D_q\omega_g}$ which decides RPL's speed of response and useful in deciding RPL control parameter K of the system.

$$K = \tau_v D_q \omega_g \tag{2.22}$$

Here, the inner loops (CCL & VCL) control system dynamics can be omitted as the bandwidths of the synchronverter and the inner loops are well separated.

The synchronverter controller generates the three-phase sinusoidal reference voltage signals for the inner voltage control loop (VCL) as per the below equation (2.23).

$$e_g = \omega_g \Psi \left[\sin\theta_g \quad \sin(\theta_g - \tfrac{2\pi}{3}) \quad \sin(\theta_g + \tfrac{2\pi}{3}) \right]^T \tag{2.23}$$

As shown in figure 2-1, the signals $E^d$and E^q are obtained using *abc* to *d-q* transformation.

2.3.5 DC Link Voltage Control

In the Voltage Source Converter (VSC), it is important to have a constant DC voltage at the DC side of the inverter. Now in a PV (Photovoltaic) system, the VSC DC side is not connected to a DC source, but it is connected to a photovoltaic system (PV system) which is a power source through a DC capacitor in between. Also, the VSC switches are not practically ideal and have losses with them. These losses are provided by the discharging of the DC link capacitor, gradually.

As per [6], the control block diagram for the DC-bus voltage controller is shown in figure 2-16.

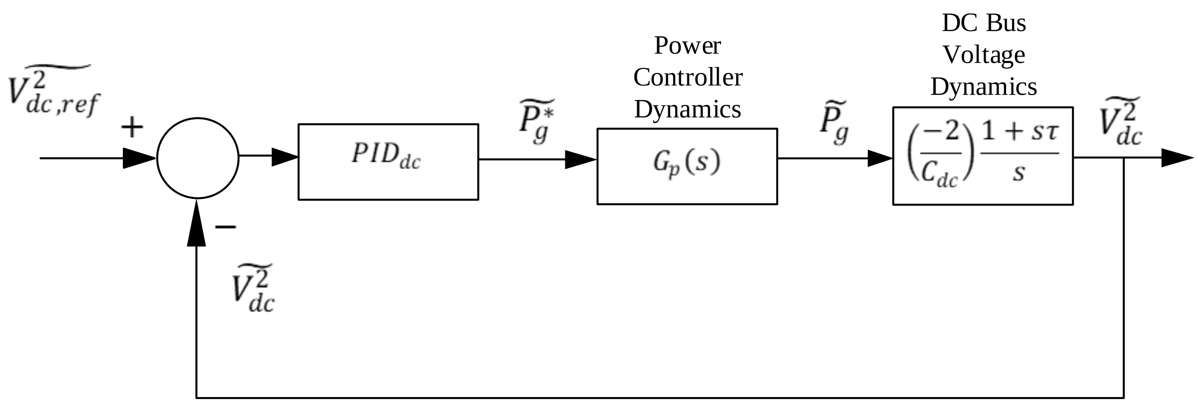

Figure 2-16: Control block diagram of the DC link voltage control

Here, C_{dc} is capacitance of the DC link capacitor which is appeared in the DC bus voltage dynamics.

$\boldsymbol{G_p(s)} = \frac{\widetilde{\boldsymbol{P_g}}}{\widetilde{\boldsymbol{P_g^*}}}$ is describing the Power Controller Dynamics which is the closed loop transfer function of the APL (Active Power Loop) of the synchronverter control system. APL is shown in figure 2-14.

Closed loop transfer function for the APL can be found as below:

$$G_p(s) = \frac{3|V_{cf}||V'_{pcc}| / X'_2\omega_g^*}{s^2 J_g + sD_p + 3|V_{cf}||V'_{pcc}| / X'_2\omega_g^*} \tag{2.24}$$

2.3.6 PCC Voltage Regulator (AC Voltage Control)

PCC Voltage regulation is an important aspect of the PV-STATCOM system for the regulation of the PCC voltage whenever needed. As PCC voltage depends on line reactance and loading conditions, PCC voltage can exceed beyond the allowable limits and hence the PCC voltage regulation is important.

As explained in section 2.3.2, the q component of PCC voltage V_{pcc-q} becomes equal to zero in steady state. Hence, PCC voltage can be controlled by just controlling V_{pcc-d}. A control block diagram for the PCC voltage Regulator is discussed in [6]. The control block diagram for the PCC voltage Regulator is shown in figure 2-17. Here the close loop transfer function of the RPL of the synchronverter $G_q(s)$ is considered.

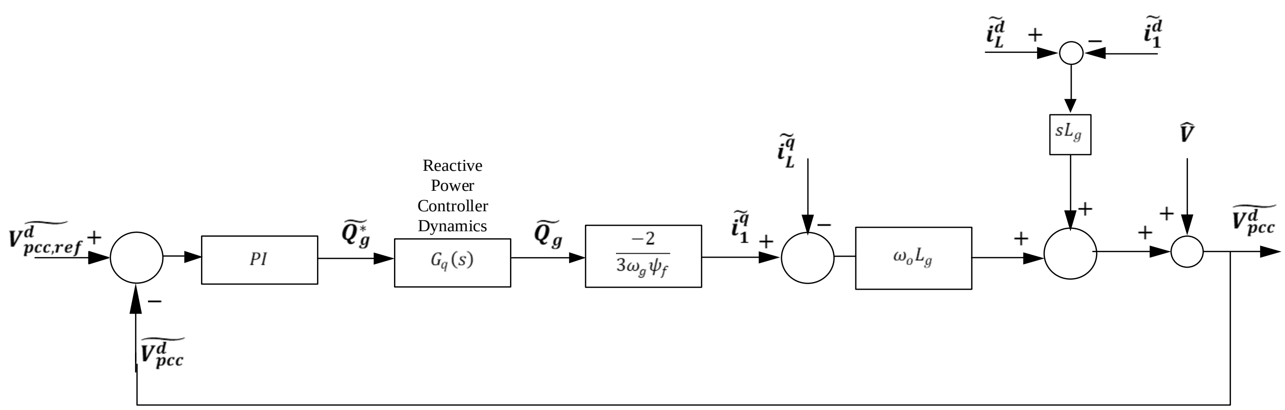

Figure 2-17: Control block diagram of PCC voltage regulator

$\boldsymbol{G_q(s)} = \frac{\widetilde{\boldsymbol{Q_g}}}{\widetilde{\boldsymbol{Q_g^*}}}$ is describing the Reactive Power Controller Dynamics which is the closed loop transfer function of the RPL (Reactive Power Loop) of the synchronverter control system. RPL is shown in figure 2-15.

Closed loop transfer function for the RPL can be found as below:

$$G_q(s) = \frac{3|V'_{pcc}|\omega_g^* D_q}{\sqrt{2}D_q X'_2 Ks + \sqrt{2}D_q^2 X'_2 \omega_g + 3\omega_g D_q V'_{pcc}} \qquad (2.25)$$

The simplified control system block diagram is shown in figure 2-18. In which

$$G_v(s) = \frac{-2}{3\omega_g \psi_f}\omega_o L_g \qquad (2.26)$$

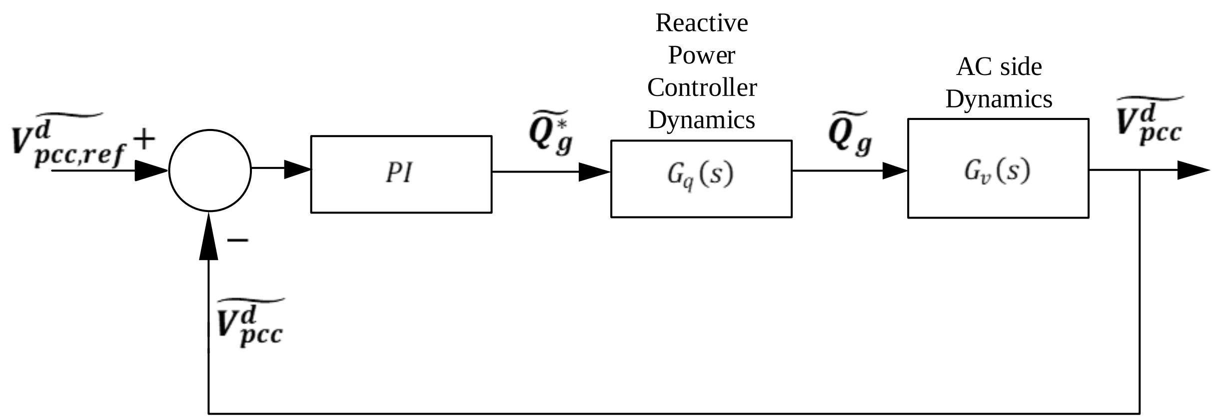

Figure 2-18: Simplified control block diagram of PCC voltage regulator

2.4 Conclusion

In this chapter the modeling of the different components of the proposed system is discussed. Proposed system consists of a PV panel, three phase 2 level inverter, LCL filter, Active and Reactive power loads and the Synchronverter-STATCOM control system. Synchronverter-STATCOM control consists of PLL (Phase Locked Loop), Inner Current control loop, Inner Voltage control loop, Synchronverter control, DC link voltage controller and PCC Voltage Regulator (AC Voltage control). The design of the whole system is discussed in the next chapter and that system is used further for the Real Time Simulation on RTDS.

Chapter 3

Control system design of the PV-STATCOM with the synchronverter control

3.1 Introduction

PV-STATCOM with synchronverter control consists of the Inner Current control loop, Inner Voltage control loop, Synchronverter control, DC link voltage controller and PCC Voltage Regulator (AC Voltage control). The procedure for the design of these various system components is described below.

3.2 Design of Phase Locked Loop (PLL)

In this section, the design of PLL is done using the principle which is explained in section 2.3.2. As shown in the figure 2-7, three-phase PCC voltages are used as the input for the PLL and *d*-*q* components are obtained using the *abc* - *d*-*q* transformation. A filter block is used to extract the DC quantity of the *q* component of PCC voltage V_{pcc-q}.

As the three phase PCC voltage signals are used as the input to the PLL block, the amplitude of the PCC phase voltage $\hat{V} = \frac{27.6\,kV}{\sqrt{3}}\sqrt{2} = 22.535$ kV. Also, Filter $G_f(s) = \frac{1}{(1+s\tau)}$ is used to filter out the higher frequency harmonics from the q component of the PCC voltage. The time constant for the filter $G_f(s)$ is $\tau = 1\,ms$ and so, the filter $G_f(s) = \frac{1}{(1+s\tau)} = \frac{1}{(1+0.001s)}$. Hence, the uncompensated loop transfer function from figure 2-8 can be written as,

$$G_{pll}(s) = \frac{\hat{V}\,G_f(s)}{s} = 22535 \times \frac{1}{(1+0.001s)} \times \frac{1}{s} \tag{3.1}$$

For choosing the required bandwidth, PI compensator is used for achieving the desired phase Crossover frequency with proper Phase Margin (PM).

As shown in the figure 2-7, the PI compensator $K_{pll} = K_p + \frac{K_i}{s}$.

K_p= 0.012 and K_i= 0.85157 are chosen for 60.2° Phase Margin (PM) at the gain crossover frequency of $270\ {}^{rad}/_{s}$.

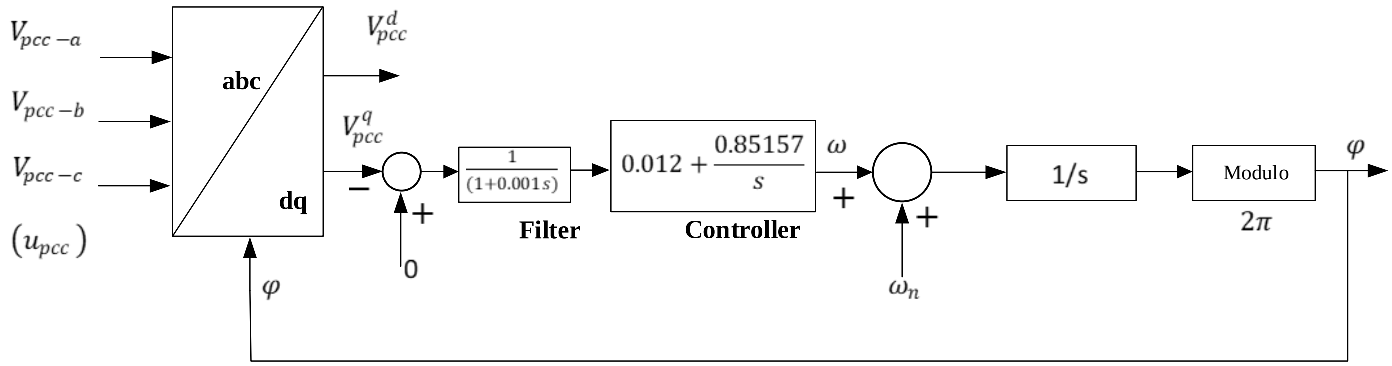

Figure 3-1: Design of PLL

The control system of PLL implemented in the simulation is shown in figure 3-1.

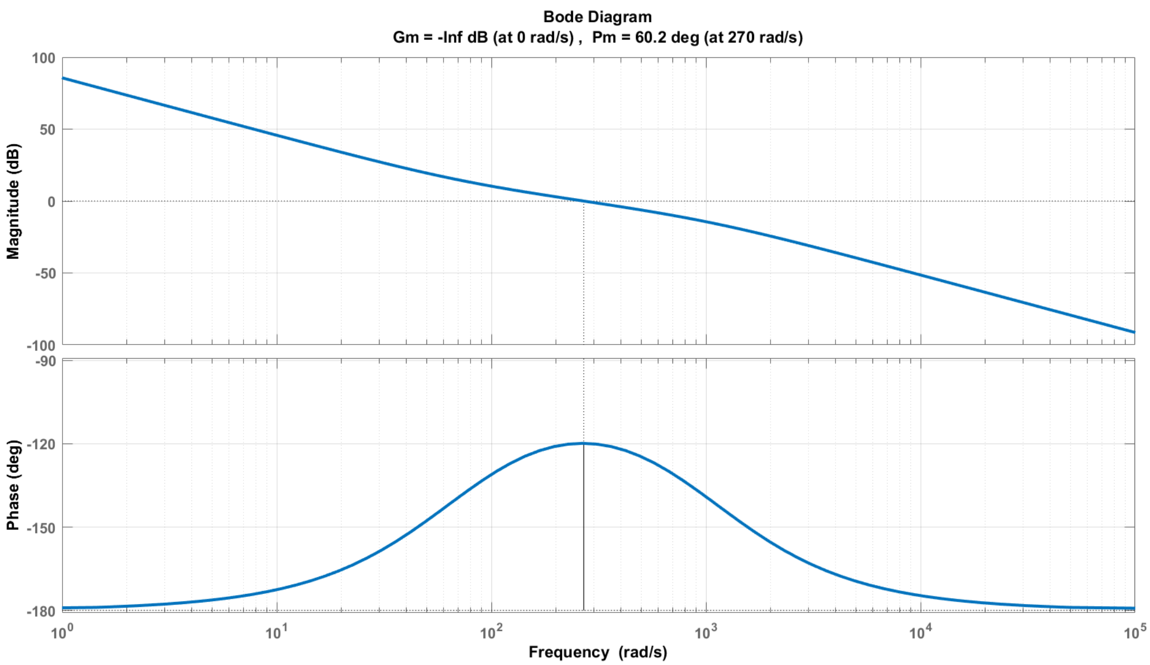

Figure 3-2: Bode plot for the compensated loop gain of PLL

In figure 3-2, the bode plot for the compensated loop gain of PLL is shown.

3.3 Design of Inner Control Loops

As discussed in the section 2.3.3, the Current Control Loop (CCL) and the Voltage Control loop (VCL) are acting as the inner control loops for the synchronverter controller. As CCL is the innermost controller, it should fastest than every control loops. VCL should be slower than CCL and faster than the synchronverter controller.

3.3.1 Current Control Loop (CCL) design

As discussed in the section 2.3.3.1, two PI compensators PI_i^d and PI_i^q are used for controlling both d and q components of the inverter output current. Also, $PI_i^d = PI_i^q = K_{pi} + \frac{K_{ii}}{s}$ .As per [6], to achieve fast response and to make the steady state error zero, it is required to design $K_{pi} = \frac{L_1}{\tau_i}$ and $K_{ii} = \frac{R_1}{\tau_i}$. The time constant of the current control loop τ_i is practically considered between 0.5 ms to 5 ms. According to the design parameters mentioned appendix, $L_1 = 40\ \mu H$ and $R_1 = 1\ m\Omega$.

Considering 1.4 ms (700 ${rad}/{s}$) time constant for the current control loop and the parameters obtained for the PI compensator are as below:

$$K_{pi} = \frac{40\times10^{-6}}{1.4\times10^{-3}} = 0.028 \quad \text{and} \quad K_{ii} = \frac{1\times10^{-3}}{1.4\times10^{-3}} = 0.714$$

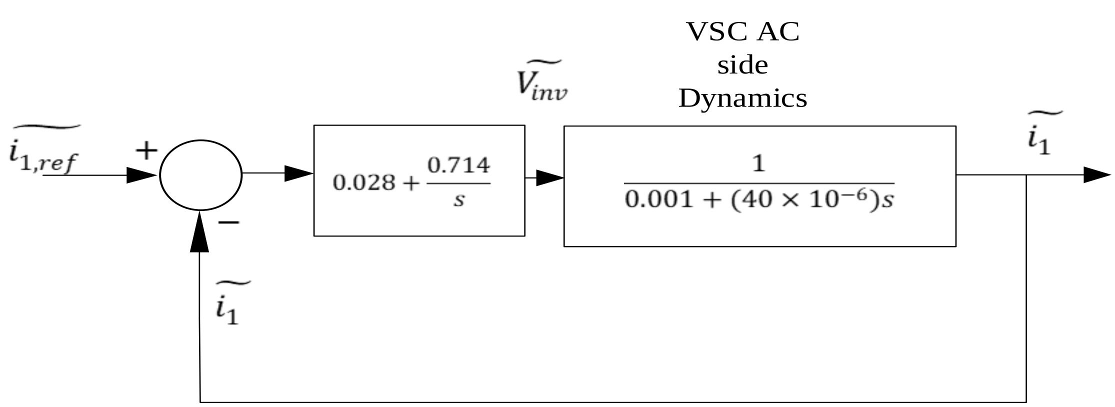

Figure 3-3: Design of inner current control loop (CCL)

As per figure 3-3, the loop gain for the current control loop is $\frac{K_{pi}s+K_{ii}}{s(R_1+sL_1)} = \frac{0.028s+0.714}{s\,(1\times10^{-3}+40\times10^{-6}\,s)}$

3.3.2 Voltage Control Loop (VCL) design

As discussed in the section 2.3.3.2, the voltage control loop (VCL) is working as the outer loop for the current control loop (CCL). Output signals of VCL act as the input signals for the CCL. Hence it is important to design the VCL slower than the CCL. As per the figure 2-11, two PI compensators PI_v^d and PI_v^q are necessary for controlling both $V_{c_f}^d$ and $V_{c_f}^q$.

Also, $PI_v^d = PI_v^q = K_{pv} + \frac{K_{iv}}{s}$. According to the design parameters mentioned in Appendix, useful parameters for the design of VCL as per figure 2-13 are: $L_1 = 40\ \mu H$ and $C_f = 700\ \mu$F.

MATLAB PID Tuner is used for the design of PI compensators which are used in the Voltage Control Loop (VCL) and the obtained parameters are as follows:

$K_{pv} = 201.097$ and $K_{iv} = 2111.754$

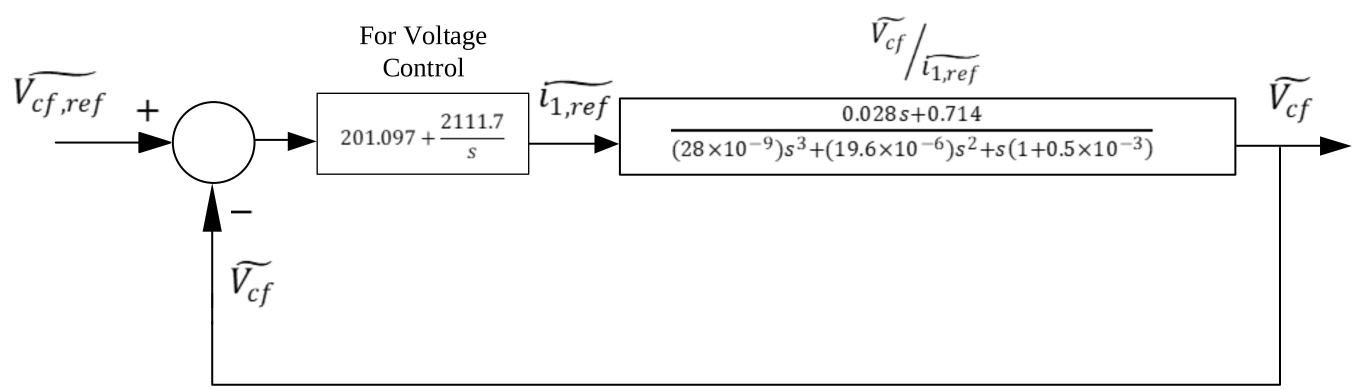

Figure 3-4: Design of inner voltage control loop (VCL)

3.4 Synchronverter design

As discussed in section 2.3.4, synchronverter has two control loops: Active power Loop (APL) and Reactive Power Loop (RPL).

As in section 2.3.4.1, APL has two main design parameters which are the frequency droop coefficient D_p and the inertia constant J_g. In the same way, as in section 2.3.4.2, RPL has the voltage droop coefficient D_q and a control parameter K which are the important design parameter.

3.4.1 Active Power Loop Design

As per section 2.3.4.1, the inertia constant is decided based on the frequency droop coefficient D_p and the APL time constant τ_f.

$$J_g = D_p \tau_f \tag{3.2}$$

Also, $D_p = {\Delta T_m}/{\Delta \omega_g}$, where ΔT_m is the amount of change in the input torque for $\Delta \omega_g$ variation in the angular speed. In this thesis, it is considered to have 100% change in torque for 0.5% change in frequency.

Also, $\Delta T_m = {\Delta P_g^*}/{\omega_N}$ 100% change in power is the rated Active Power which is 8.5 MW for the system used in this thesis.

Hence, $\Delta T_m = {8.5 \times 10^6}/{2 \times \pi \times 50} = 27056.3632$ and $\Delta \omega_g = 0.5\% \; of \; (2 \times \pi \times 50)$

$D_p = {27056.3632}/{(0.005 \times 2 \times \pi \times 50)} = 17224.63.$

Hence required D_p is 17224.63 ${N \cdot m}/{rad/sec}$

Now, considering APL time constant τ_f = 10 ms, then, the Inertia constant

$J_g = 17224.63 \times (10 \times 10^{-3})$ = 172.2463 ${N \cdot m}/{rad/sec^2}$

3.4.2 Reactive Power Loop Design

As per section 2.3.4.2, the RPL control parameter K is decided based on the voltage droop coefficient D_q and the RPL time constant τ_V.

$$K = D_q \tau_v \omega_N \tag{3.3}$$

Here, D_q = ${}^{\Delta Qg}\!/_{\Delta U_t}$, ΔQ_g is the amount of change in the input reactive power for ΔU_t difference in the synchronverter output voltage from U_t^*, where U_t^* is the nominal voltage amplitude=230$\sqrt{2}$ V.

In this thesis, it is considered to have 100% change in Reactive Power for 10% of the nominal voltage.

100% change in reactive power is the rated capacity which is 8.5 MVAR for this thesis.

So, $\Delta U_t = 10\%\ of\ 230\sqrt{2}\,\text{V} = 32.526\ \text{V}$ and $D_q = {}^{8.5 \times 10^6}\!\Big/_{0.1 \times 230\sqrt{2}} = 261329.4\ {}^{MVAR}\!/_{V}$

Hence required D_q is 261329.4 ${}^{MVAR}\!/_{V}$

Now, considering RPL time constant τ_v = 10 ms, then, RPL control parameter $K = 261329.4 \times 0.01 \times 314.159 = 8.21 \times 10^5\ {}^{MVAR \cdot rad}\!/_{V}$

3.5 DC link Voltage Control Design

As discussed in the section 2.3.5, according to figure 2-16, the DC link voltage control loop consists of the power controller dynamics $G_p(s)$ and the DC bus voltage dynamics.

Hence the uncompensated DC link voltage control loop gain

$$H_{dc,uncomp} = \left(\frac{-2}{C_{dc}}\right)\frac{1+s\tau}{s}G_p(s)\text{, where } G_p(s) = \frac{{}^{3|V_{cf}||V'_{pcc}|}\!\Big/_{X'_2\omega_g^*}}{s^2 J_g + sD_p + {}^{3|V_{cf}||V'_{pcc}|}\!\Big/_{X'_2\omega_g^*}}$$

$$H_{dc,uncomp} = \left(\frac{-2}{C_{dc}}\right)\frac{1+s\tau}{s}\frac{{3|V_{cf}||V'_{pcc}|}/{X'_2\omega_g^*}}{s^2 J_g + sD_p + {3|V_{cf}||V'_{pcc}|}/{X'_2\omega_g^*}}\,\omega_N \tag{3.4}$$

For the system parameters mentioned in Appendix, the bode plot for $H_{dc,uncomp}$ is shown below in figure 3-5.

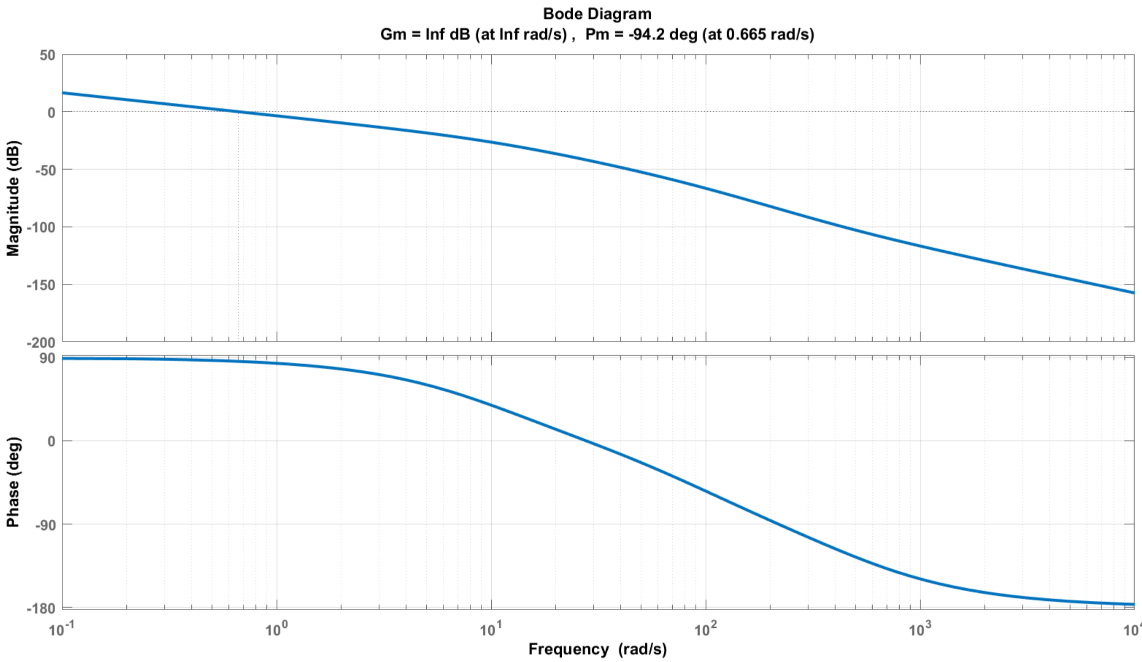

Figure 3-5: Bode plot for the uncompensated loop gain of DC link voltage control

The uncompensated loop gain $H_{dc,uncomp}$ has Phase Margin (PM) = -94.2° , which is showing the unstable system. For appropriate phase margin at the desired gain cross over frequency PID compensator is used.

Bandwidth of the DC link voltage control loop should be considered less than the bandwidth of the Active Power Loop (APL) which is the inner loop for the DC link voltage control loop.

PID compensator is as below for 60° phase margin (PM) at 50 ${rad}/{s}$ bandwidth.

PID= -34.632 $\frac{(1+0.21s)(1+1.1s)}{s(1+(1.59\times10^{-5})s)}$

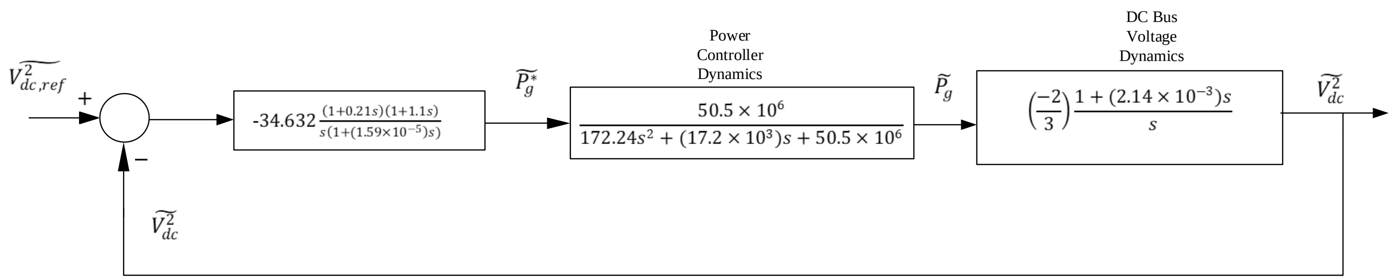

Figure 3-6: Design of DC link voltage control loop

From figure 2-16, the compensated DC link voltage control loop gain is $H_{dc,comp} = PID\left(\frac{-2}{C_{dc}}\right)\frac{1+s\tau}{s}G_p(s)$, which is shown in figure 3-6 mathematically. Bode plot for the same is shown in the figure 3-7.

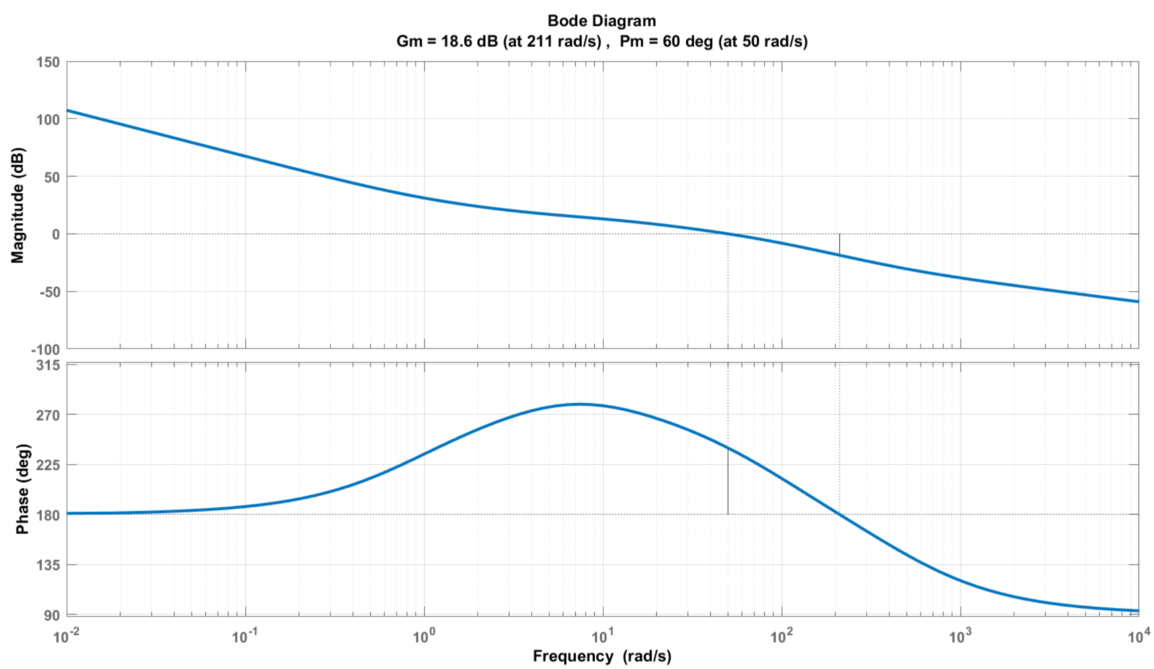

Figure 3-7: Bode plot for the compensated loop gain of DC link voltage control

3.6 PCC Voltage Regulator (AC Voltage Control)

The modeling and the control loop diagram for the PCC voltage regulator are discussed in section 2.3.6.

As shown in figure 2-18, the PI compensator is useful in providing appropriate DC gain to the uncompensated loop gain of the system to achieve zero steady state error and disturbance rejection.

As in figure 2-18, the compensated loop gain is $PI \times \frac{-2}{3\omega_g \psi_f}\omega_o L_g \frac{3|V'_{pcc}|\omega_g^* D_q}{\sqrt{2}D_q X'_2 K s + \sqrt{2}D_q^2 X'_2 \omega_g + 3\omega_g D_q V'_{pcc}}$

Useful system parameters for the design of PI compensator using the above expression are mentioned in the Appendix. Here, MATLAB Control System Designer tool is used for the tuning of the PI compensator which is shown below.

$$PI = 20851.2 + \frac{1.1584 \times 10^9}{s}$$

The compensated loop gain can be found from figure 3-8. Values of parameters which are used to obtain below gains, are stated in Appendix.

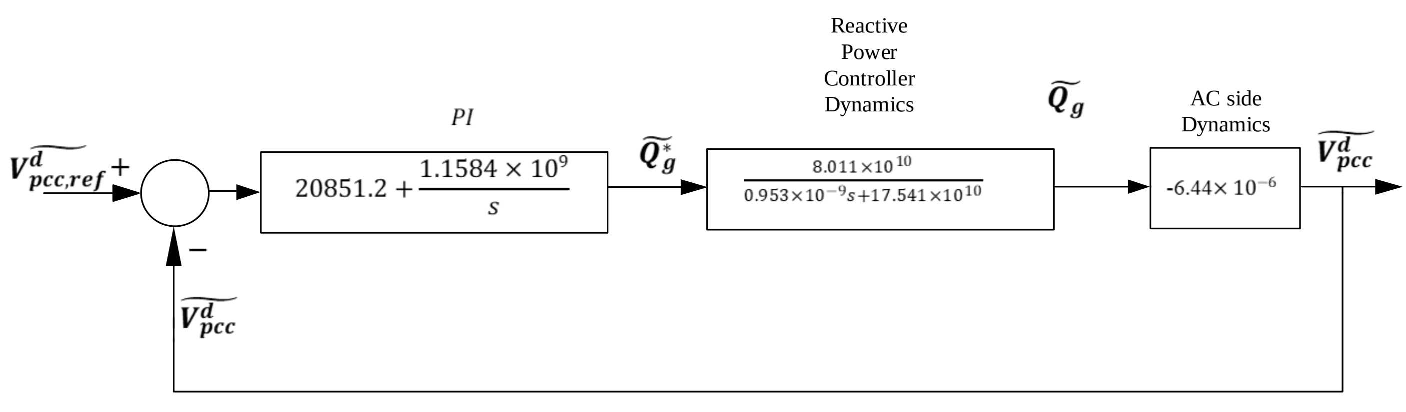

Figure 3-8: Design of PCC voltage control loop

3.7 Conclusion

In this chapter the control system design of the PV-STATCOM with synchronverter controller has been discussed in detail. These parameters are used for the simulation of the whole system on RTDS. The Real Time Simulation results are in the next chapter.

Chapter 4

Real Time Digital Simulation Results

4.1 Introduction

This chapter is presenting the Real-Time simulation results of the proposed PV-STATCOM system with the synchronverter controller. The system consists a grid connected 8.5 MVA inverter system with the PV source. Various active and reactive power loads are connected to the Point of Common Coupling (PCC) to study the system in different conditions.

4.2 Concept of Real Time Digital Simulation

Various simulation software is available to perform the simulation of the power systems and power electronics in non-real time. During these simulations, several complex differential equations are needed to be solved and so this non-real time simulation takes more time to simulate the whole system than the time taken by the real phenomenon.

For these reasons, Real Time Simulation is becoming more popular in Power Systems and Power Electronics simulation studies. Real time simulation provides more accurate and reliable simulation studies than non-real simulation.

In this thesis, Real Time Digital Simulator (RTDS) developed by the RTDS Technologies has been used for real time simulation studies. RTDS is specialized parallel processing hardware to simulate the power system and power electronics models and real time using its high-speed processors. Various models understudies can be implemented on the RTDS by use of its Graphical User Interface (GUI) software RSCAD.

In this study all the components of the power system, various loads, power electronics inverter, PV model and controller are implemented on RTDS using the RSCAD.

4.3 Real Time Digital Simulator (RTDS)

RTDS is the real time power system simulator by RTDS technologies. It has the state-of-the-art POWER8TM processor from IBM. This powerful multicore processor makes faster and more capable than the RTDS Simulator's previous processing hardware. RTDS chassis has 2-3 times the simulation capacity of a fully-loaded PB5 based rack. It can solve hundreds of nodes on a single core. It provides up to 50% reduced timesteps for the high precision simulations. RTDS allows licensing of 1 to 10 cores per chassis and can provide full connectivity up to 60 chassis. RTDS has various Input/Output (I/O) cards such as Giga Transceiver Digital Input (GTDI), Giga Transceiver Analog output (GTAO), Giga Transceiver Analog input (GTAI), Giga Transceiver Digital Output (GTDO) which are useful for communication with external devices like DSP boards or microprocessor. This feature is useful for Hardware-In-Loop (HIL) simulations [16]. The system under study is modelled in RSCAD-Draft and then the RSCAD-Runtime feature is used to upload it on RTDS processor cards after compilation. RSCAD-Runtime is useful in monitoring the currents, voltages and various control signals. Also, it is used to give commands like connect/disconnect using switches and buttons, use of sliders, etc. during the real time simulation.

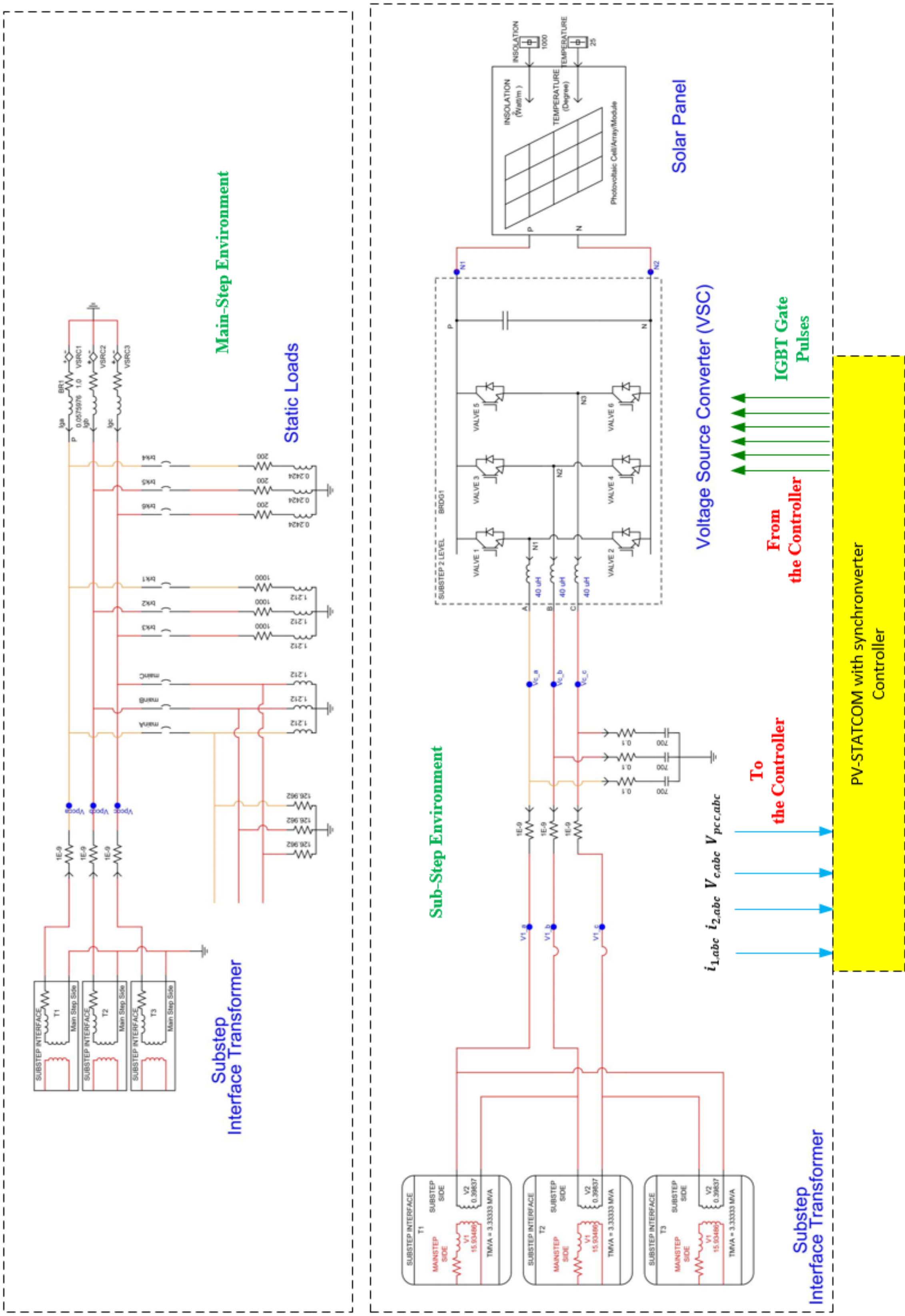

Figure 4-1: Power Circuit of PV-STATCOM with synchronverter control in RSCAD

4.4 Real Time Digital Simulation Study Results

In this study the 8.5 MVA grid connected PV system is used with different loads at the point of common coupling (PCC). The grid is considered as an infinite source of 27.6 kV rated voltage (line to line RMS). Hence, the amplitude of phase voltage 22.5 kV which is considered as the nominal value for the voltage at PCC. The whole structure of the system is shown in figure 2-1. Various parameters of the system are mentioned in the Appendix.

The following studies have been done for the performance evaluation of the proposed system:

1) Full PV mode: Proposed system acts as Conventional PV system in forward power flow as well as in the reverse power flow condition.

2) Partial STATCOM mode: Proposed system acts as PV-STATCOM for voltage control using remaining MVA capacity for reactive power flow.

3) Full STATCOM mode: Proposed system acts as a STATCOM for voltage control operation without active power generation.

4.4.1 Full PV Mode

Full PV mode is a conventional PV Operation. As in a conventional grid-connected PV system, in full PV mode, PV-STATCOM injects the whole amount of generated PV power into the grid. In this mode remaining inverter MVA capacity after active power generation remains unused. Hence, the system is underutilized during the full PV mode operation. The impact of PV power generation variation on the PCC voltage is also analyzed during this study.

It consists of two Power flow conditions:

1. Forward Power Flow condition

2. Reverse Power Flow condition

4.4.1.1 Forward Power Flow condition

As per figure 2-1, the inverter system and the grid both can provide active power to the load connected at the PCC (Point-of-Common Coupling). If the active power generation by the PV-inverter system is less than the active power requirements of the load then the remaining active power is provided by the grid. This condition is called the "Forward Power Flow" condition. In the Forward Power Flow condition, the active power flow is from grid to the PCC.

For the Full PV mode, the constant impedance loads of rating 6 MW active and 2 MVAR reactive at 27.6 kV rated voltage (line to line RMS) are connected at the PCC.

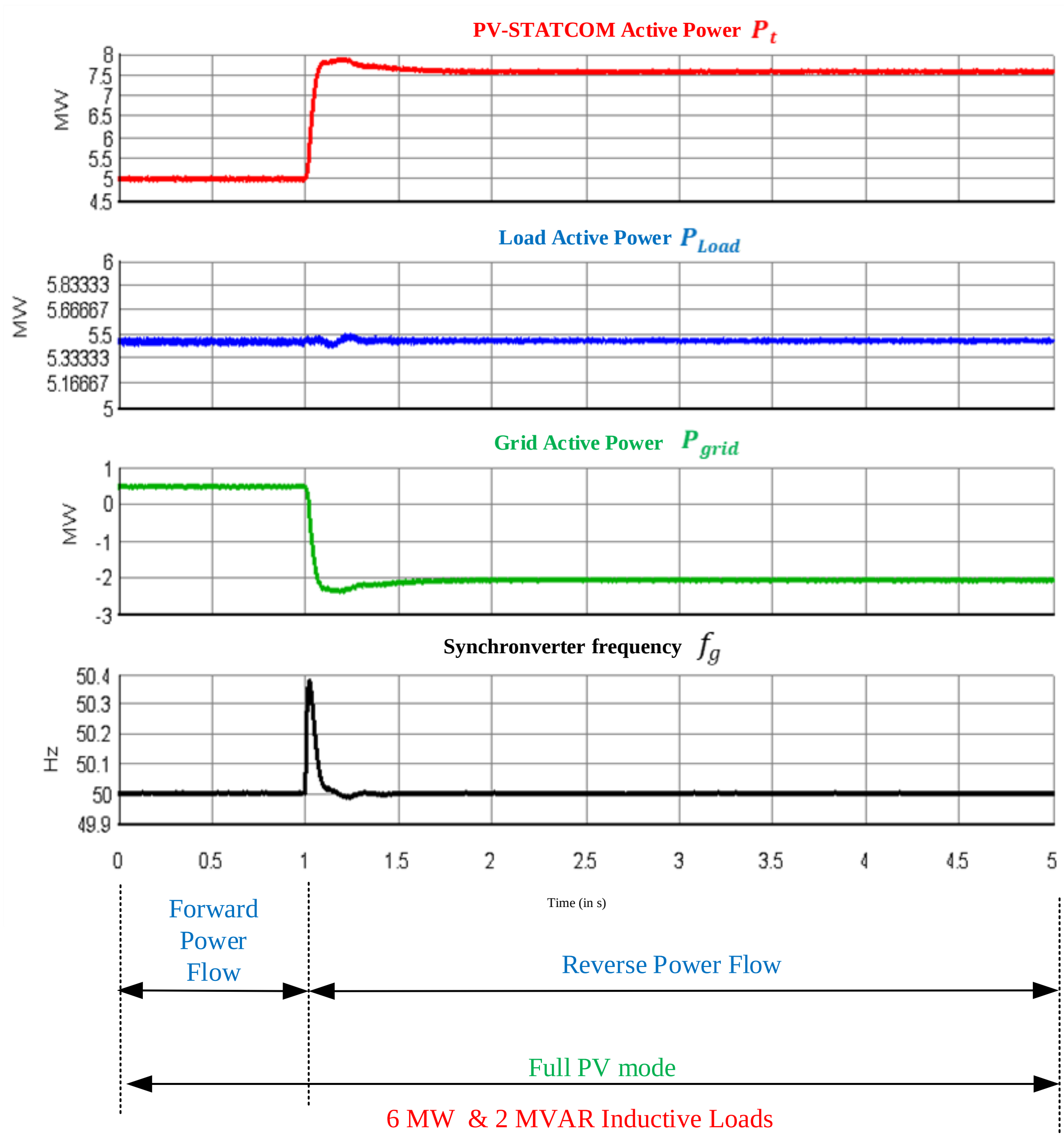

Figure 4-2: Simulation results of full PV mode in forward power flow condition

For t = 0 to t=1 second, 5 MW amount of active power is generated by the PV system as shown in figure 4-2. At this time the PCC voltage (Phase voltage amplitude V_{pcc}^{d}) is around 21.4 kV as in figure 4-3. At this voltage the active power requirement of the load is around 5.4 MW evident in figure 4-2. As PV is providing 5 MW active power, the remaining 0.4 MW is provided by the grid to the load. Hence this is the "Forward Power Flow" condition.

4.4.1.2 Reverse Power Flow condition

As discussed in section 2.2.1, PV power generation depends on the solar irradiation. As solar irradiation increases solar power increases. In this case, PV power generation is increased to 7.5 MW from 5 MW, by changing the irradiance in the PV model.

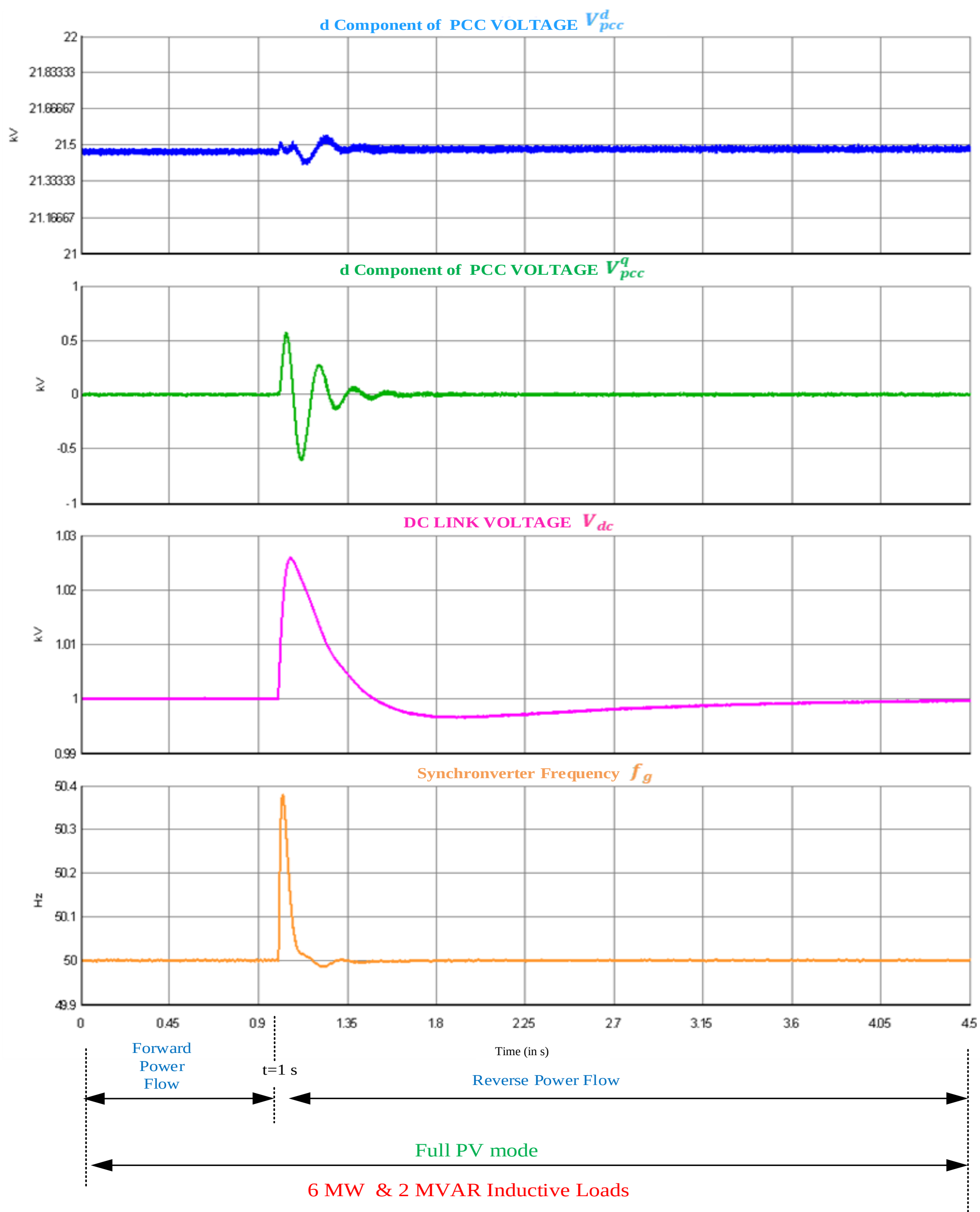

Figure 4-3: Simulation results of full PV mode in reverse power flow condition

At t=1 second, the PV power generation is changed and increased to 7.5 MW. As more active power is injected into the PCC, the PCC voltage is slightly increased to 21.5 kV as shown in figure 4-3.

As PV system is generating 7.5 MW and load requirement is 5.4 MW, the remaining active power is absorbed by the grid as shown in figure 4-2 and so P_{grid} is around -2 MW. Hence this is the "Reverse Power Flow" condition.

During the transient at t=1 second, as solar irradiance is increased suddenly, the power generation by PV is also increased suddenly. As generation is increased suddenly as per the behavior of the synchronverter, synchronverter frequency is also increased as shown in figure 4-2.

Also, the DC link capacitor gets charge due to the sudden power generation at PV side and DC link voltage increases as in figure 4-3. To bring back the increased frequency, synchronverter electromagnetic torque T_e increases and consequently PV-STATCOM active power output P_t also increases, as in figure 4-2, and it follows the increased power generated from PV. Hence, the synchronverter frequency start falling back towards 50 Hz. DC link capacitor also gets discharged by the DC link voltage controller's action which is evident in figure 4-3. Hence, in this way after the smooth transient, synchronverter frequency come back to 50 Hz as shown in figures 4-1 and 4-2.

In figure 4-4, 3-phase load currents, grid currents and PV-STATCOM currents are shown during the transition between Full-PV mode to Full STATCOM mode.

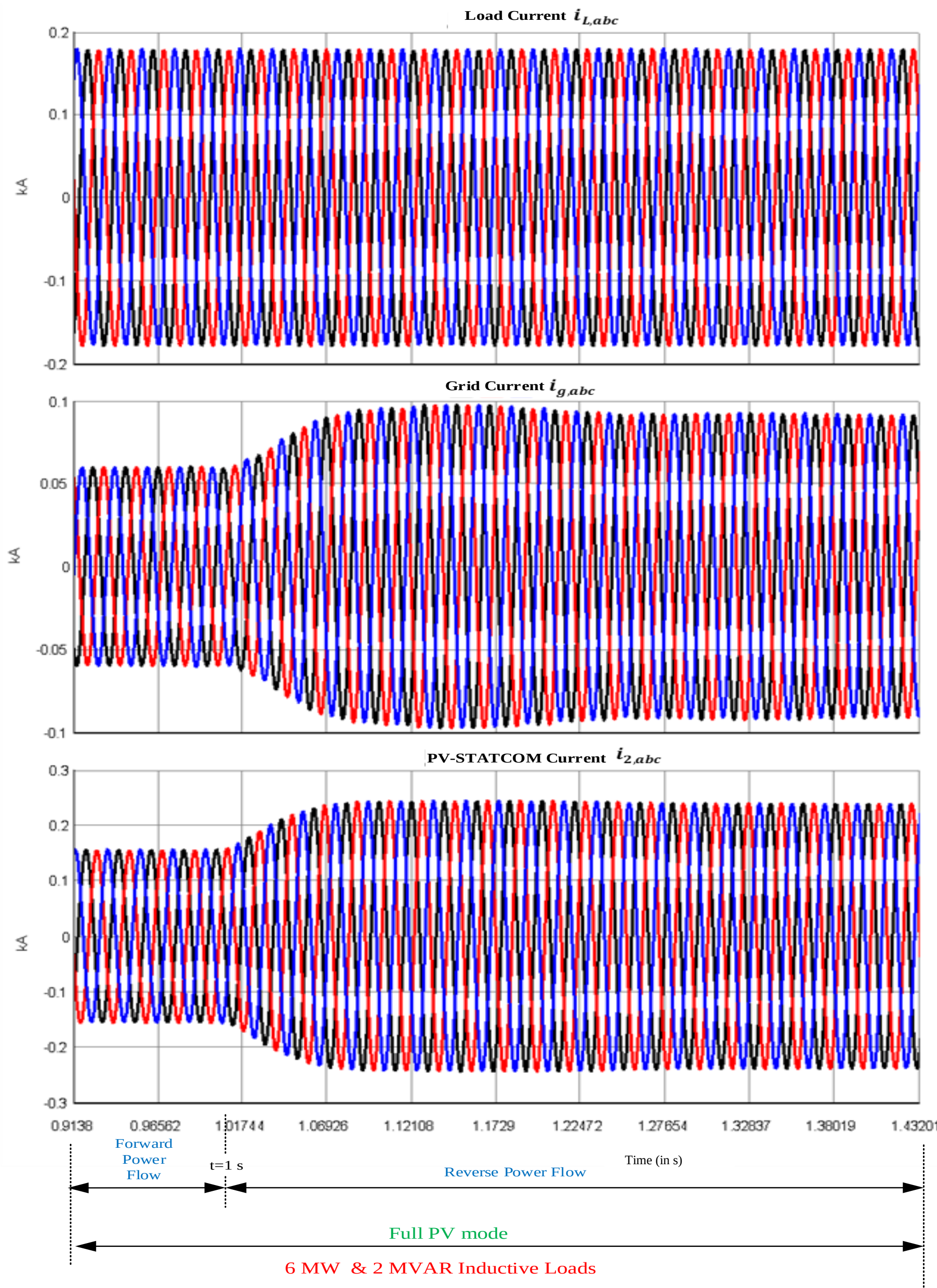

Figure 4-4: Simulation results of currents in full PV mode

4.4.2 Partial STATCOM Mode

Power generation through PV panels is highly intermittent and varies according to the variations in solar irradiance and temperature conditions as shown in figures 2-1 and 2-2. Hence most of the time in a day, the PV system's MVA capacity (inverter MVA rating) is underutilized. In PV-STATCOM, after delivery of the generated active power, the remaining MVA capacity can be used for the reactive power exchange. This mode of operation is called the "Partial STATCOM mode". In this thesis, the Partial STATCOM mode is used for the PCC voltage regulation through the required reactive power exchange.

In this thesis, two different cases are considered for the simulation study of Partial STACTCOM mode:

1) Effect of PCC Voltage Reference variation
2) Effect of load variation

4.4.2.1 Effect of PCC Voltage Reference variation

In this study, the constant impedance loads of rating 6 MW resistive and 2 MVAR inductive at 27.6 kV rated voltage (line to line RMS) are connected at the PCC. In starting the PV system is working in the Full PV mode. In full PV mode, the PCC voltage regulator is not being used and the reactive power reference Q_g^* is set to zero value and so the synchronverter output reactive power Q_g is also zero. Hence, the reactive power requirement of the filter capacitor and the inductance of coupling transformer is provided by the grid, which is evident from the slight negative value of Q_t in figure 4-7. During the Full PV mode PV power generation is 5 MW and the amplitude of phase voltage at PCC V_{pcc-d} is around 21.5 kV. The q component of PCC voltage V_{pcc-q} is maintained at zero by PLL. DC link voltage V_{dc} is 1000 V. Synchronverter frequency f_g is at 50Hz. Load is consuming 5.5 MW of active power at present value of PCC voltage. Out of which, 5 MW is provided by the PV system and 0.5 MW is provided by the grid, hence it is the forward power flow. As shown in figure 4-5, the PCC voltage control enable signal is showing the status of $V_{pcc,ref}^d$. Table 4-1 indicates different values of $V_{pcc,ref}^d$ for different levels of control signal.

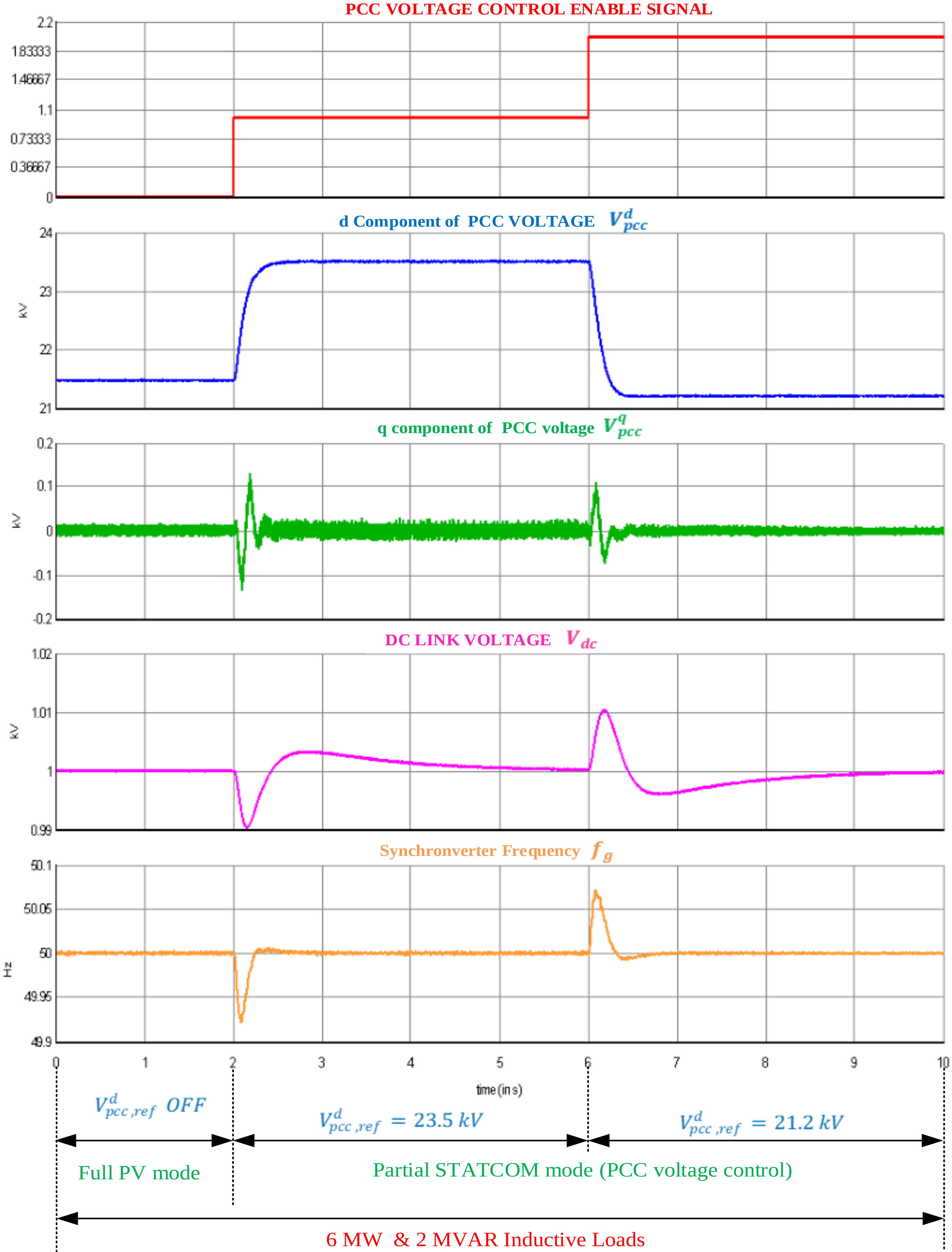

Figure 4-5: Simulation results of voltage and frequency in partial STATCOM mode with PCC voltage reference variation

At t=2 second; the PCC voltage regulator is enabled and $V_{pcc,ref}^{d}$=23.5 kV is selected. To track this new PCC voltage-reference an appropriate reactive power reference is generated. As shown in figure 4-7, the PV-STATCOM is providing approximately 4 MVAR of reactive power and acting as a Capacitor, which is the "capacitive mode operation" of the PV-STATCOM.

Table 4.1: PCC reference voltages for different control signals

PCC voltage control enable signal	$V_{pcc,ref}^{d}$
0	Disabled
1	23.5 kV
2	21.2 kV

Also, PCC voltage is increased and settled at 23.5 kV from 21.5 kV as shown in figure 4-5. Due to change in the PCC voltage the active and reactive power requirements of the load are also changed. Due to the increment in active power requirement of the load after t=2 sec as shown in figure 4-6, the synchronverter frequency falls in starting. According to the synchronverter active power droop control shown in figure 2-1, because of the fall in ω_g, synchronverter electromagnetic torque T_e and consequently PV-STATCOM active power output increases. As the power generation at the PV side is not changed, this sudden power output increment is provided by the DC link capacitor and so DC link capacitor discharges and V_{dc} falls as in figure 4-5. To charge back the DC link capacitor, the DC link controller reduces the power output of the PV-STATCOM by reduction in P_g^* and so DC link capacitor gets charged by the PV power output. After the smooth transient synchronverter frequency come back to 50 Hz as shown in figure 4-5. PV-STATCOM output settles back to 5 MW in steady state as there is no change in solar power generation.

At t=6 second, $V_{pcc,ref}^{d}$ is changed to 21.2 kV. To track the new PCC voltage reactive power reference Q_g^* is changed to negative by PCC voltage regulator and PV-STATCOM absorbs the reactive power and acts as an inductor. Hence, the PV-STATCOM operates in the "Inductive mode operation".

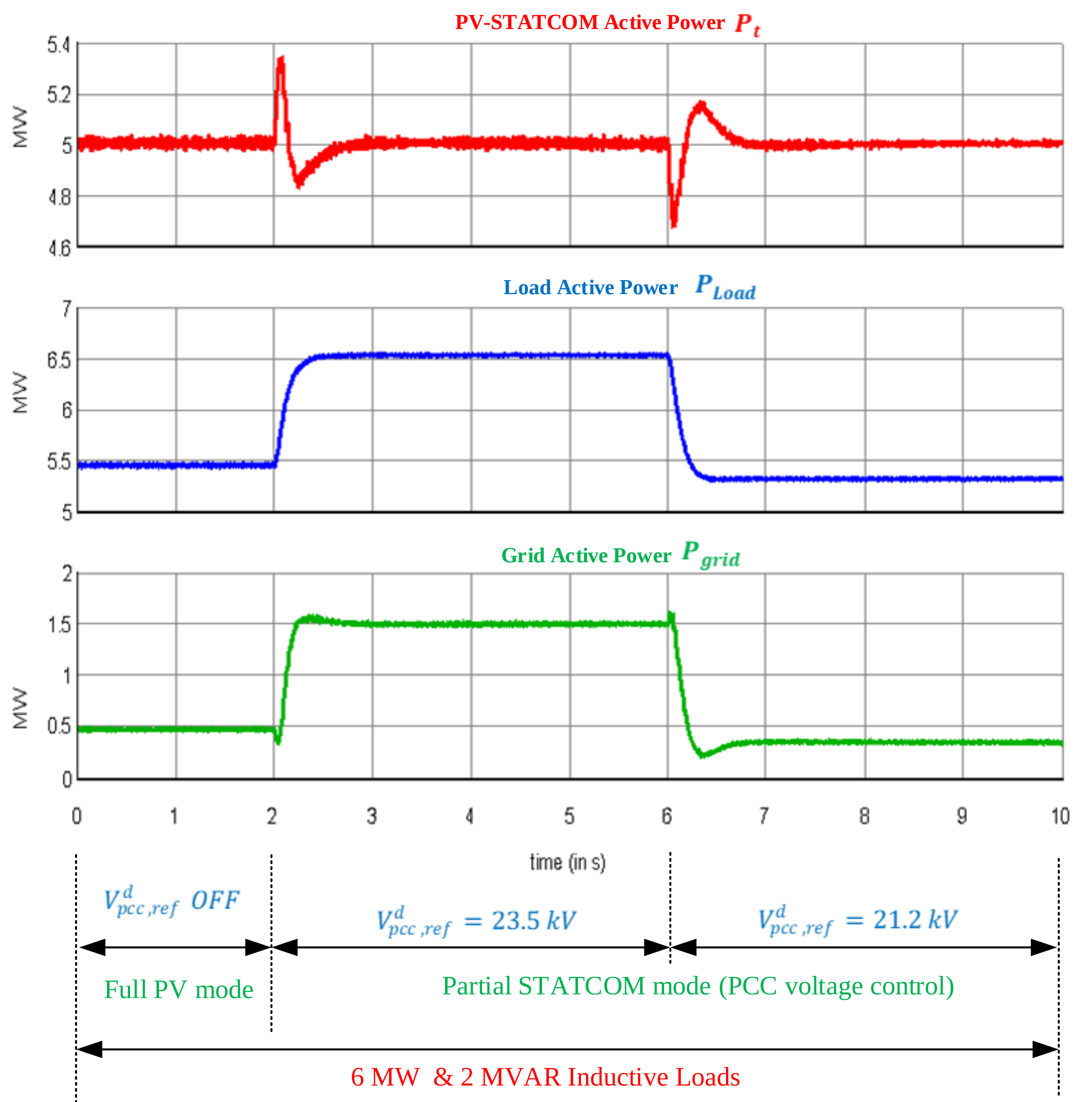

Figure 4-6: Simulation results of active powers in partial STATCOM mode with PCC voltage reference variation

PCC voltage is decreased and settled at 21.2 kV from 23.5 kV as shown in figure 4-5. Due to change in the PCC voltage the active and reactive power requirements of the load are also changed. Decrement in the active power has impact on the synchronverter frequency at t= 6 second as shown in figure 4-5. According to active power droop characteristic, PV-STATCOM active power output decreases and DC link capacitor gets charged up. Due to the DC link controller action, PV-STATCOM active power is increased and settle back to the 5 MW in steady state. Also, after smooth transient, synchronverter frequency settles to 50 Hz.

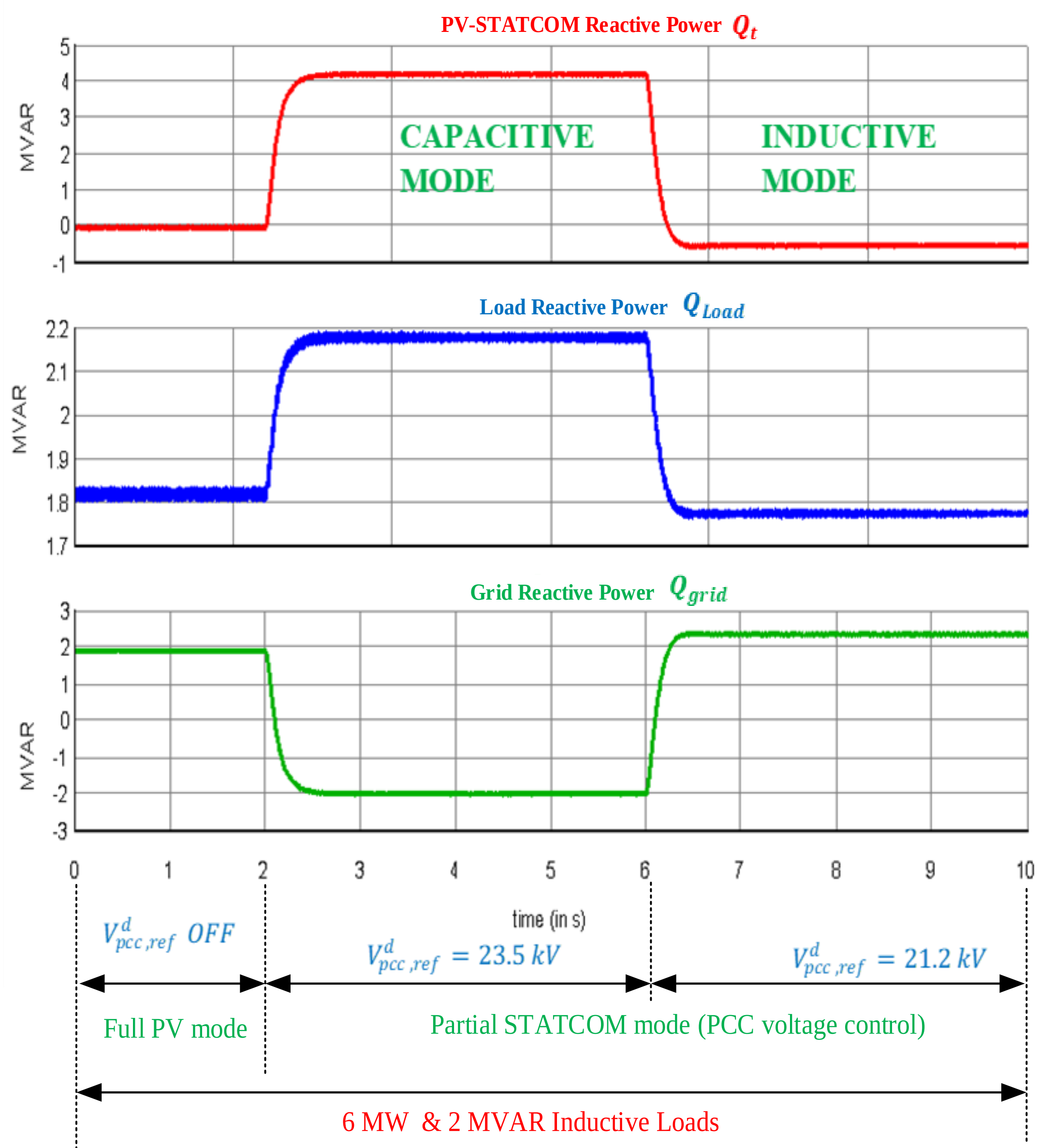

Figure 4-7: Simulation results of reactive powers in partial STATCOM mode with PCC voltage reference variation

4.4.2.2 Effect of load variation

In starting of this study, the constant impedance loads of rating 6 MW resistive and 2 MVAR inductive at 27.6 kV rated voltage (line to line RMS) are connected at the PCC. Also, all other starting conditions are same as in previous section 4.4.2.1.

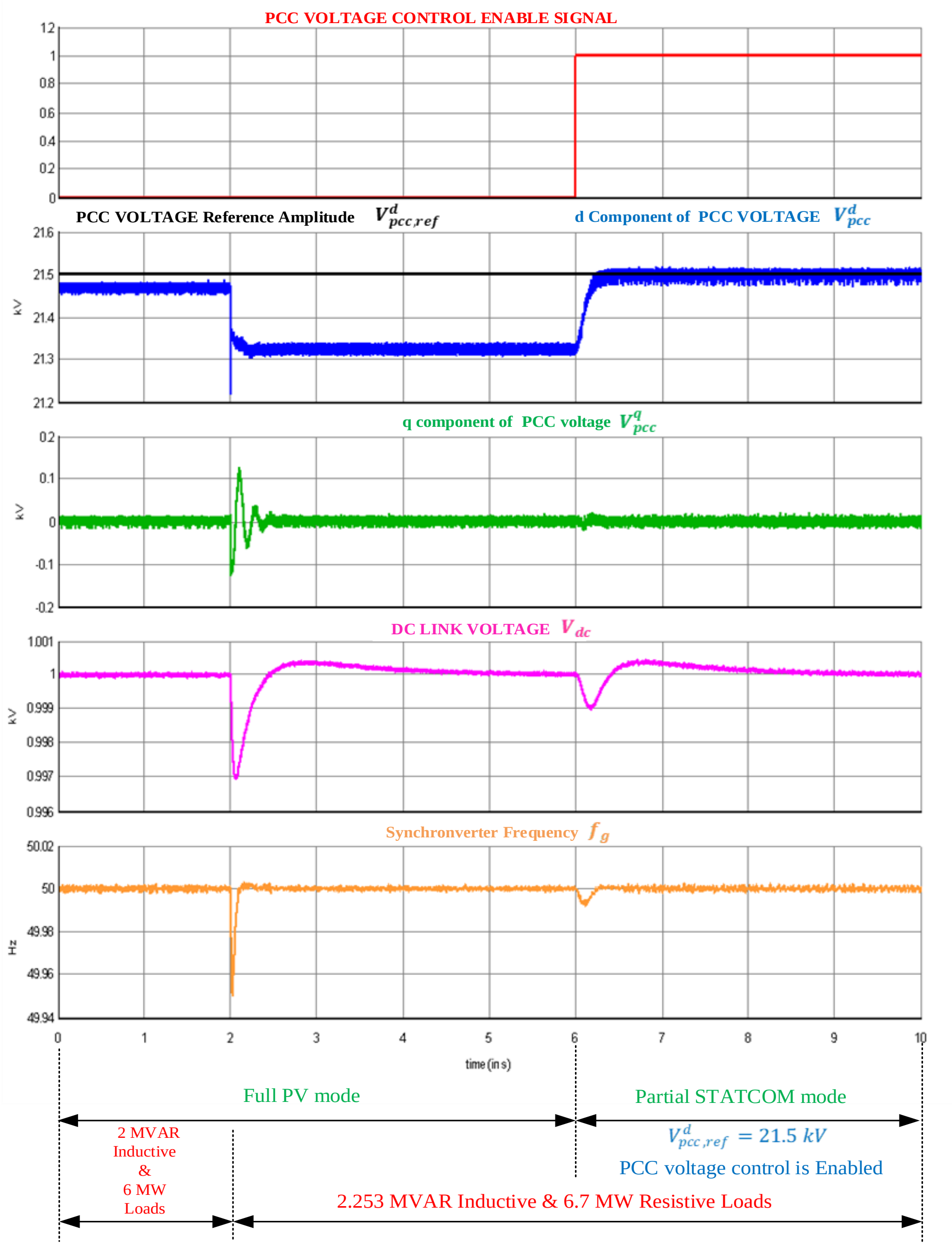

Figure 4-8: Simulation results of voltage and frequency in partial STATCOM mode

with load variation

For t=0 to t=2 second, PV STATCOM is in Full PV mode and the load requirement is around 5.5 MW and 1.8 MVAR at PCC. The reactive power requirement of the load is provided by the grid. Active power generation by PV is 5 MW and the PCC voltage is around 21.5 kV.

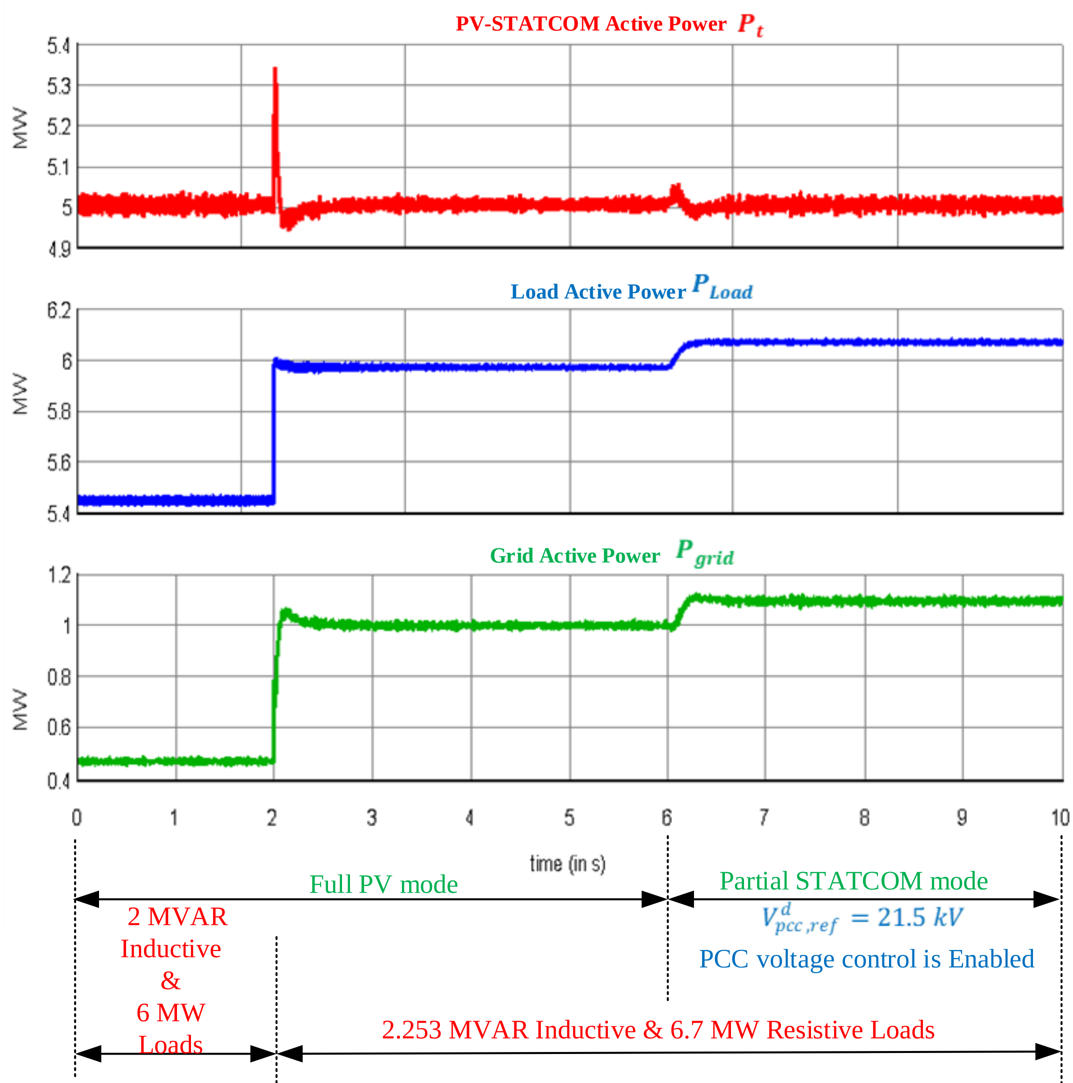

Figure 4-9: Simulation results of active powers in partial STATCOM mode with load variation

At t=2 second, an RL load of 0.7115 MVA (at 27.6 kV), (1000 + j380.76) Ω/phase, is connected at the PCC. Hence the total load at PCC is 2.253 MVAR and 6.7 MW (for 27.6 kV). Due to RL load connection, PCC voltage falls around 21.3 kV which is evident in figure 4-8. Due to change in the PCC voltage the active and reactive power requirements of the load are also changed. Also, synchronverter frequency, DC link voltage, active and reactive power output of PV-STATCOM go through the transients according to the synchronverter dynamics described in the previous section and also settle down to the former values in steady state.

Here it is evident that the PCC voltage is changing with the change in load at PCC and the PCC voltage is needed to be regulated against the load variations at the PCC.

At t=6 seconds, PCC voltage regulator is enabled and the PV-STATCOM enters into the Partial STATCOM mode from the Full PV mode. As $V_{pcc,ref}^{d}$=21.5 kV, PV-STATCOM acts as a capacitor and inject sufficient amount of the reactive power into the PCC to increase the PCC voltage to 21.5 kV as shown in figure 4-10 and figure 4-8 respectively.

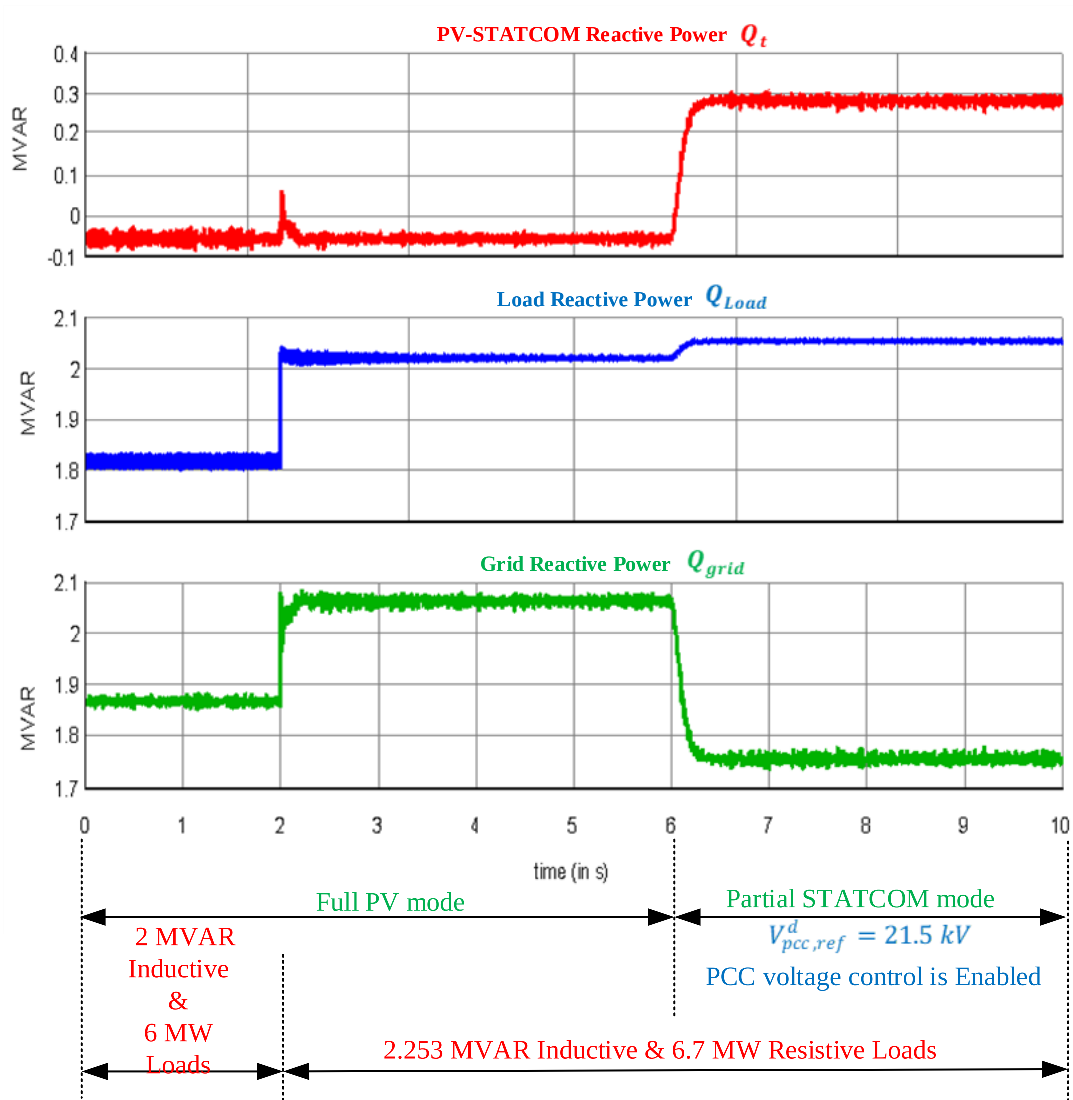

Figure 4-10: Simulation results of reactive powers in partial STATCOM mode with load variation

4.4.3 Full STATCOM Mode

During the nighttime, there is no power generation from the PV source. During this time the whole MVA capacity of the inverter can be used for the reactive power exchange and to maintain the PCC voltage within the permissible limits. Also, during the conditions like large transients or faults, the PV-STATCOM system can be switched to the Full STATCOM mode from the normal full PV mode or Partial STATCOM mode immediately. In Full STATCOM mode, PV is disconnected from the PV-STATCOM system and then the whole MVA capacity can be used for the PCC voltage support.

In starting of this study, the constant impedance loads of rating 6 MW resistive and 2 MVAR inductive at 27.6 kV rated voltage (line to line RMS) are connected at the PCC. Also, all other starting conditions are same as in previous section 4.4.2.1.

For t=0 to t=1.4 second, PV STATCOM is in Full PV mode and the load requirement is around 5.5 MW and 1.8 MVAR at PCC. The reactive power requirement of the load is provided by the grid. Active power generation by PV is 5 MW and the PCC voltage is around 21.5 kV.

At t=1.4 second, a large RL load is connected at the PCC. Due to large load the PCC voltage falls below 21 kV as in figure 4-11.

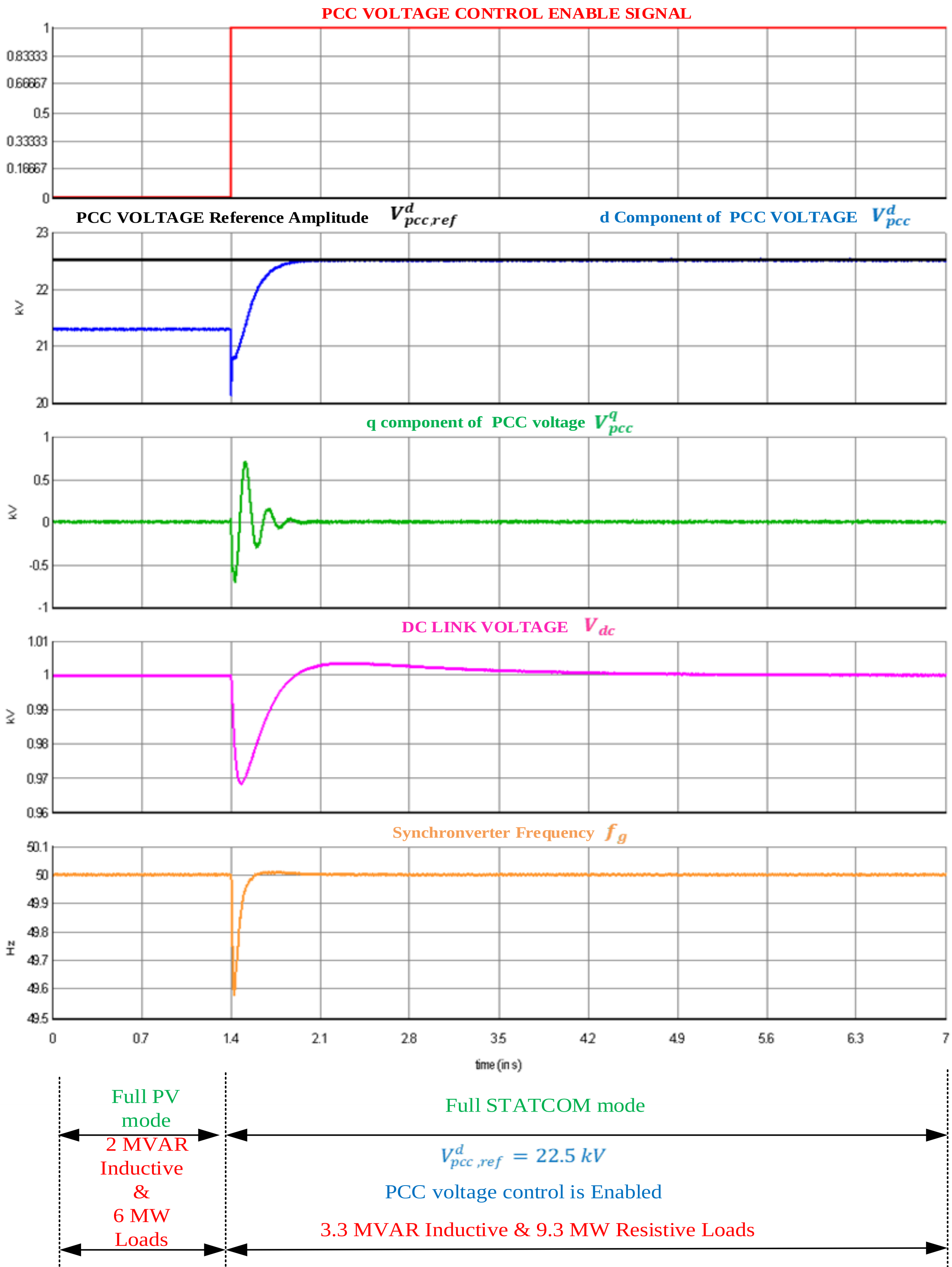

Figure 4-11: Simulation results of voltage and frequency for Full STATCOM

In this thesis, 21 kV PCC voltage is considered as the minimum permissible amplitude of PCC phase voltage. Hence suddenly, the PV is disconnected from the inverter (in the simulation PV is disconnected virtually by making the value of irradiance minimum, which is virtual disconnection) and the PCC voltage controller is enabled. Now entire inverter MVA capacity can be used for the reactive power exchange, which is called Full-STATCOM mode.

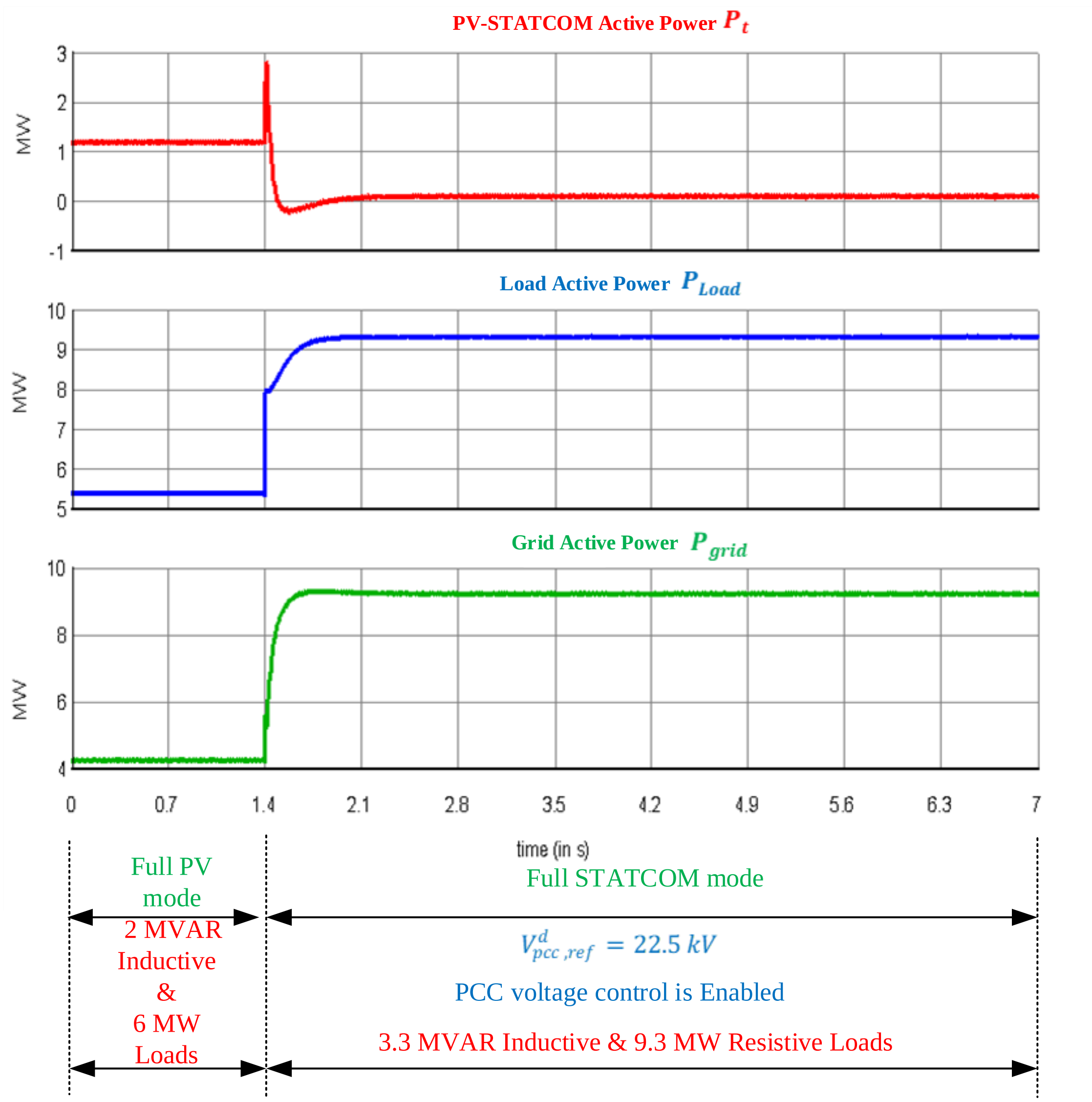

Figure 4-12: Simulation results of active powers for Full STATCOM

As shown in the figure 4-13, around 5 MVAR of reactive power is provided by the PV-STATCOM. Also, synchronverter frequency, DC link voltage, active and reactive power output of PV-STATCOM go through the transients according to the synchronverter dynamics.

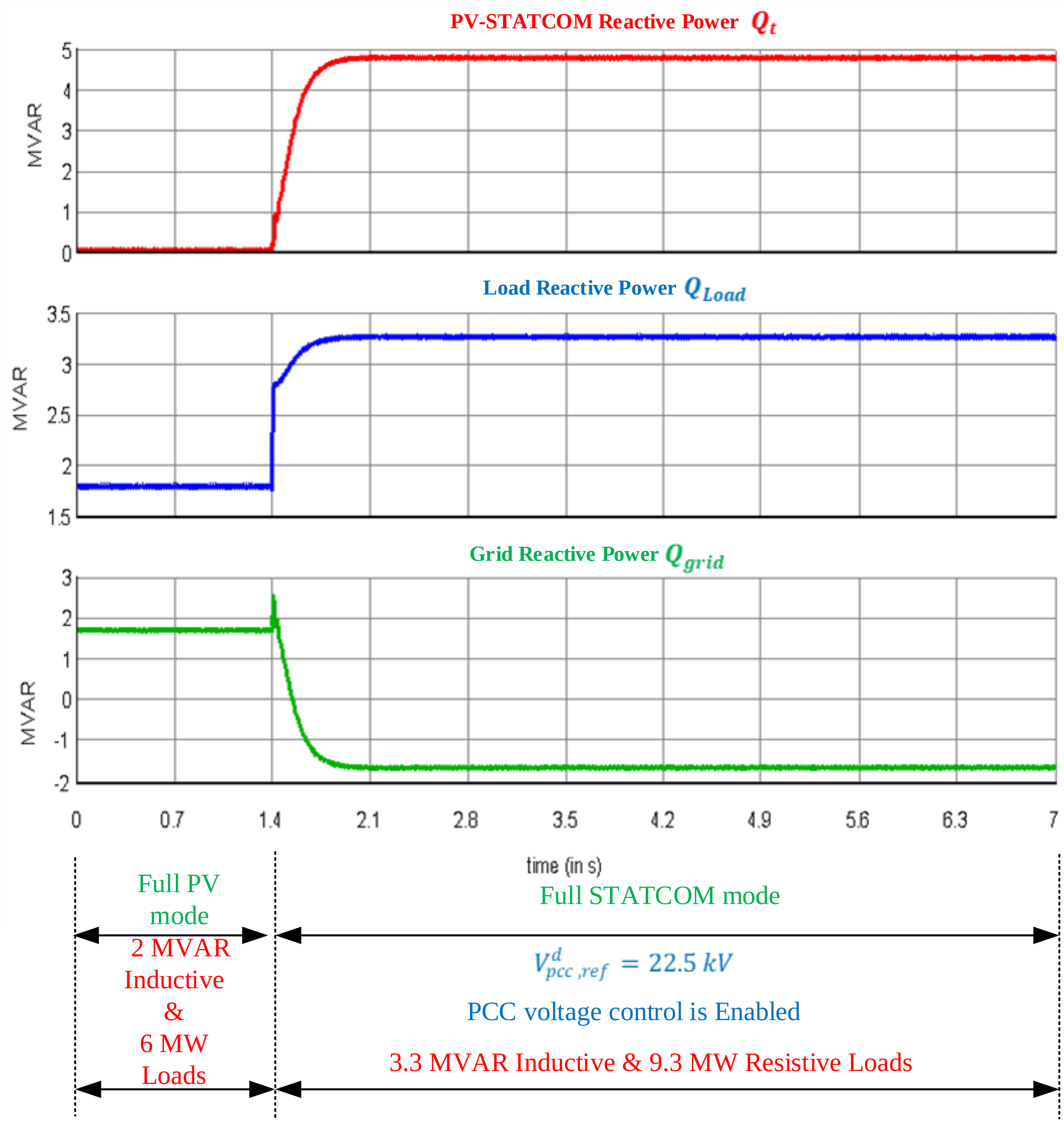

Figure 4-13: Simulation results of reactive powers for Full STATCOM

In figure 4-14, 3-phase load currents, grid currents, PV-STATCOM currents and PCC voltages are shown during the transition between Full-PV mode to Full STATCOM mode.

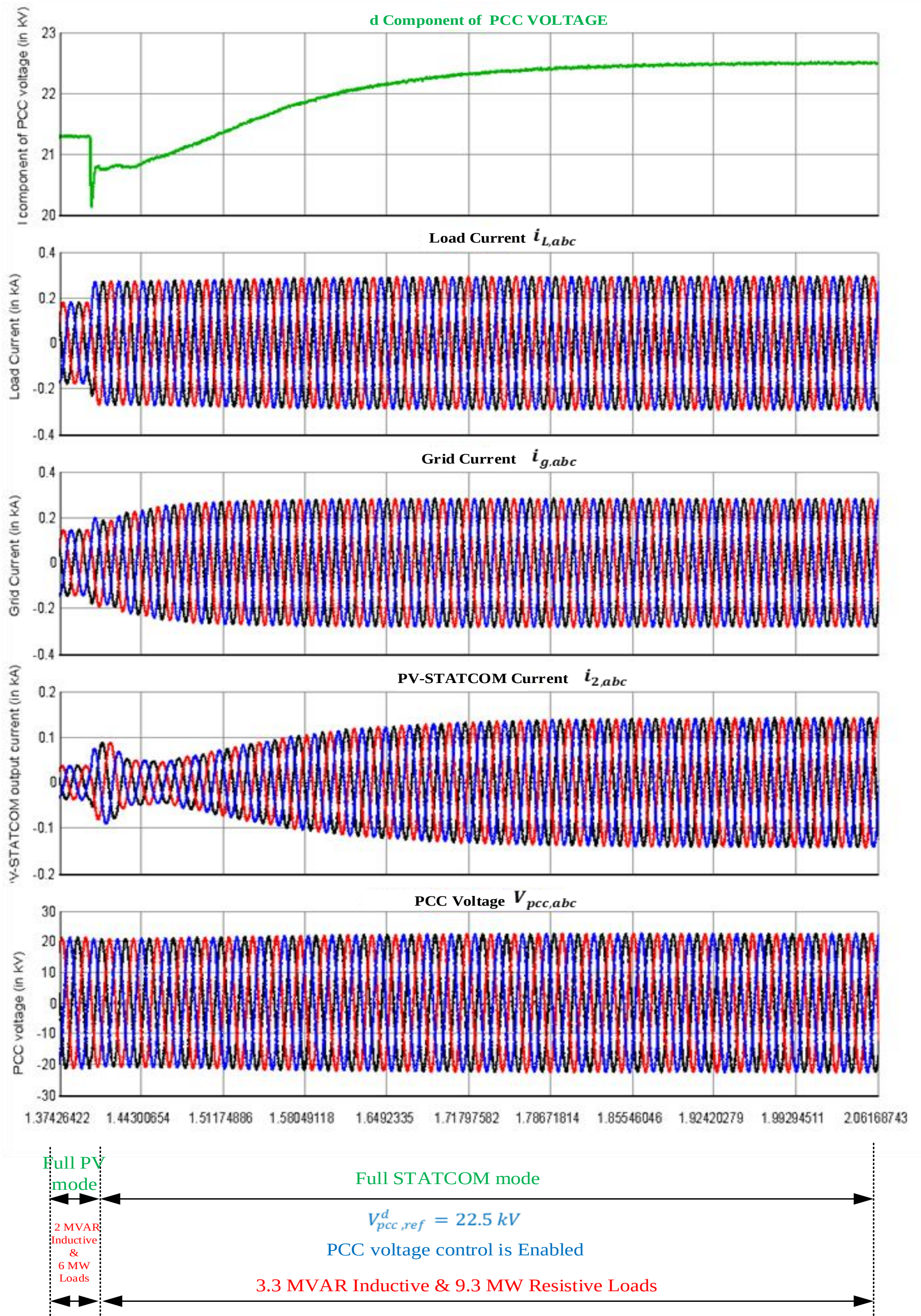

Figure 4-14: Simulation results of voltage and currents for Full STATCOM

4.5 Conclusion

In this chapter, the 8.5 MVA grid connected PV system has been simulated in real time using RTDS. Total three modes of operation: Full PV mode, Partial STATCOM mode and Full STATCOM mode, have been discussed and their results have been shown. The effect of synchronverter control has been shown in the PV-STATCOM system. In Full PV mode, the proposed system only provides the active power to the grid and loads. It is found that the impact of change in power generation on the system's frequency (synchronverter frequency) is less oscillatory and following the characteristic of the synchronous generator by virtual inertia. In Partial STATCOM mode, the proposed system is regulating the PCC voltage by exchanging the reactive power from the remaining VA capacity of the inverter after injecting the generated active power from PV. In full STATCOM mode, the PV is disconnected and the whole VA capacity of the inverter is used for the PCC voltage regulation. Full STATCOM mode is useful at night time and also during the emergency cases like fault or severe voltage fluctuations. The design of the PV-STATCOM system with synchronverter control has been validated using these real time simulation results.

Chapter 5

Conclusions and Future Scope

Conventional grid-connected PV solar system has an inverter that converts DC power into AC power and generally consists of a conventional current controller scheme. It is understood in chapter 1 that this type of conventional PV inverter system is not reliable for the era of renewable energy sources and Distributed Generation systems. The need for an advanced inverter system like synchronverter with inner control loops has been stated in 1st chapter. Also, it is understood that the PV-STATCOM system is important for fully utilizing the inverter VA capacity and providing voltage support to the PCC.

Chapter 2 and chapter 3 consist of modeling and design of various control loops of the PV-STATCOM system with synchronverter control. The whole control system is designed for the *d-q* reference frame (Rotating Reference Frame) control. Classical control theory is used for the various control loop design. MATLAB's Control System Toolbox is also used for the design of the inner voltage control loop compensator.

In chapter 4 the PV-STATCOM system with synchronverter control is validated for different modes of operation using RTDS for real-time simulation. In Full PV mode, the proposed system only provides the active power to the grid and loads. It is found that the impact of change in power generation on the system's frequency (synchronverter frequency) is less oscillatory and following the characteristic of the synchronous generator by virtual inertia. In Partial STATCOM mode, the proposed system is regulating the PCC voltage by exchanging the reactive power from the remaining VA capacity of the inverter after injecting the generated active power from PV. In full STATCOM mode, the PV is disconnected and the whole VA capacity of the inverter is used for the PCC voltage regulation. Full STATCOM mode is useful at night time and also during the emergency cases like fault or severe voltage fluctuations.

Hence, in this thesis, a combined system consists of the synchronverter control and PV-STATCOM system has been discussed. Here it has been tried to implement the Virtual Inertia concept in the PV-STATCOM system.

The outcome of this thesis is the design of a grid-connected PV system with virtual inertia support and droop control, active and reactive power control and better voltage regulation profile with efficient use of the PV inverter.

Future scope related to the "PV-STATCOM with synchronverter control" may be as follows:

- State Space Modeling of "PV-STATCOM with synchronverter control" system

- Effect of variation in the parameters like inertia constant J_g, frequency droop coefficient D_p, voltage droop coefficient D_q, RPL control parameter K and DC link capacitor C_{dc}, on the small signal stability of PV-STATCOM in different modes of operation

- Study of the impact of bandwidth on PCC voltage regulation and dc link voltage control

- Parallel operation of two or more "PV-STATCOM with synchronverter control" system

APPENDIX

A.1 Grid Parameters

Grid voltage V_g	27.6 kV
Grid side inductance L_g	57.6 mH
Grid side resistance R_g	1 Ω

A.2 PV Panel Parameters

Open circuit voltage of a panel	36.9 V
Short circuit current of a panel	8.43 A
Number of panels in series	34
Number of panels in parallel	1095
Voltage of a panel at MPP	29.62 V
Current of a panel at MPP	7.7668 A

A.3 PV Inverter Parameters

IGBT ON State Resistance R_{ON}	0.0001 Ω
IGBT Off State Resistance R_{OFF}	$1.0e^{6}$ Ω
IGBT Forward Voltage Drop V_{fd}	0 V
Snubber Resistance $R_{snubber}$	6600 Ω
Snubber Capacitance $C_{snubber}$	0.001 μF
DC link Capacitor C_{dc}	3 F
DC link Voltage V_{dc}	1000 V

A.4 Filter and Isolation Transformer Parameters

Inverter side Inductor L_1	$40\mu H$
Filter Capacitance C_f	$700\ \mu F$
Rating of the Isolation transformer	8.5 MVA
Leakage Inductance of Isolation transformer L_2 (referred to primary winding)	$10\mu H$
Winding Connection and Voltage level of isolation transformer	Delta (398.37 V)/Star-Ground (27.6 kV)

REFERENCES

[1] "IEEE Recommended Criteria for Terrestrial Photovoltaic Power Systems," in ANSI/IEEE Std 928-1986, vol., no., pp.0_1-, 1986, doi: 10.1109/IEEESTD.1986.79644.

[2] Widalys De Soto, SA Klein, and WA Beckman, "Improvement and Validation of a Model for Photovoltaic Array Performance," in *Solar energy*, vol. 80 Issue 1, pp. 78-88, 2006

[3] G. H. Kim, Y. J. Kim, M. Park, I. K. Yu, and B. M. Song, "RTDS-based Real Time Simulations of Grid-Connected Wind Turbine Generator Systems," *IEEE 2010 Applied Power Electronics Conference (APEC),* Feb. 22-25, 2010, pp. 2085 -2090.

[4] R. K. Varma and E. M. Siavashi, "PV-STATCOM: A New Smart Inverter for Voltage Control in Distribution Systems," in IEEE Transactions on Sustainable Energy, vol. 9, no. 4, pp. 1681-1691, Oct. 2018, doi: 10.1109/TSTE.2018.2808601.

[5] B. Liu and B. Song, "Modeling and Analysis of an LCL Filter for Grid-Connected Inverters in Wind Power Generation Systems," 2011 IEEE Power and Energy Society General Meeting, 2011, pp. 1-6, doi: 10.1109/PES.2011.6039828.

[6] Amirnaser Yazdani and Reza Iravani, Voltage-Sourced Converters in Power Systems: Modeling, Control, and Applications: John Wiley & Sons, 2010.

[7] A. Timbus, R. Teodorescu, F. Blaabjerg, and M. Liserre. "Synchronization Methods for Three Phase Distributed Power Generation Systems. An Overview and Evaluation." In Power Electronics Specialists Conference, 2005. PESC '05. IEEE 36th, pages 2474–2481, 16-16 June 2005.

[8] M. Ciobotaru, R. Teodorescu, P. Rodriguez, A. Timbus, and F. Blaabjerg. "Online Grid Impedance Estimation for Single-Phase Grid-Connected Systems Using PQ Variations." In Power Electronics Specialists Conference, 2007. PESC 2007. IEEE, pages 2306–2312, 17-21 June 2007.

[9] Z. Qu, J. C. -H. Peng, H. Yang and D. Srinivasan, "Modeling and Analysis of Inner Controls Effects on Damping and Synchronizing Torque Components in VSG-Controlled Converter," in IEEE Transactions on Energy Conversion, vol. 36, no. 1, pp. 488-499, March 2021, doi: 10.1109/TEC.2020.3010049.

[10] Z. Shuai, C. Shen, X. Liu, Z. Li and s. John Shen, "Transient Angle Stability of Virtual Synchronous Generators Using Lyapunov's Direct Method," *IEEE Trans. Smart Grid*, vol. 10, no. 4, pp. 4648-4661, July 2019.

[11] Moon Won Sik, Hur Jae-Sun, and Kim Jae-Chul, "A Protection of Interconnection Transformer for DG In Korea Distribution Power System," in *Power and Energy Society General Meeting, 2012 IEEE*, 2012, pp. 1-5.

[12] N. Pogaku, M. Prodanovic and T. C. Green, "Modeling, Analysis and Testing of Autonomous Operation of an Inverter-Based Microgrid," in IEEE Transactions on Power Electronics, vol. 22, no. 2, pp. 613-625, March 2007, doi: 10.1109/TPEL.2006.890003.

[13] S. Dong and Y. C. Chen, "Adjusting Synchronverter Dynamic Response Speed via Damping Correction Loop," in IEEE Transactions on Energy Conversion, vol. 32, no. 2, pp. 608-619, June 2017, doi: 10.1109/TEC.2016.2645450.

[14] Q. Zhong and G. Weiss, "Synchronverters: Inverters That Mimic Synchronous Generators," in IEEE Transactions on Industrial Electronics, vol. 58, no. 4, pp. 1259-1267, April 2011, doi: 10.1109/TIE.2010.2048839.

[15] H. Wu et al., "Small-Signal Modeling and Parameters Design for Virtual Synchronous Generators," in IEEE Transactions on Industrial Electronics, vol. 63, no. 7, pp. 4292-4303, July 2016, doi: 10.1109/TIE.2016.2543181.

[16] RTDS Hardware Manual, "Rev. 2," *RTDS Technologies, Winnipeg, MB*, pp. 13.1-13.19, 2012.

[17] H. P. Beck and R. Hesse, “Virtual Synchronous Machine,” in Proc. 9th Int. Conf. Elect. Power Quality Utilisation, 2007, pp. 1–6.

[18] M. Ashabani and Y.-R. Mohamed, “Novel Comprehensive Control Framework for Incorporating Vscs to Smart Power Grids Using Bidirectional Synchronous-VSC,” IEEE Trans. Power Syst., vol. 29, no. 2, pp. 943–957, Mar. 2014.

[19] S. D’Arco and J. A. Suul, “Virtual Synchronous Machines-Classification of Implementations and Analysis of Equivalence To Droop Controllers For Microgrids,” in Proc. IEEE PowerTech Grenoble, 2013, pp. 1–7.

[20] J. Alipoor, Y. Miura, and T. Ise, “Power System Stabilization Using Virtual Synchronous Generator with Alternating Moment of Inertia,” IEEE J. Emerg. Sel. Top. Power Electron., vol. 3, no. 2, pp. 451–458, Jun. 2015.

[21] J. Liu, Y. Miura, H. Bevrani, and T. Ise, “Enhanced Virtual Synchronous Generator Control for Parallel Inverters in Microgrids,” IEEE Trans. Smart Grid, to be published, doi: 10.1109/TSG.2016.2521405.

[22] F. Katiraei and J. R. Agüero, "Solar PV Integration Challenges," in IEEE Power and Energy Magazine, vol. 9, no. 3, pp. 62-71, May-June 2011, doi: 10.1109/MPE.2011.940579.

[23] C. L. Masters, "Voltage Rise: The Big Issue When Connecting Embedded Generation to Long 11 kV Overhead Lines," in Power Engineering Journal, vol. 16, no. 1, pp. 5-12, Feb. 2002, doi: 10.1049/pe:20020101.

[24] Hingorani, Narain G., and Laszlo Gyugyi. “Understanding FACTS: Concepts and Technology of Flexible AC Transmission Systems”. IEEE Press, 2000.

[25] Digambar M. Tagare, "Distributed Generation (DG) and Distributed Resources (DR)," in Electricity Power Generation: The Changing Dimensions, IEEE, 2011, pp.275-299, doi: 10.1002/9780470872659.ch14.

[26] J. Rocabert, A. Luna, F. Blaabjerg and P. Rodríguez, "Control of Power Converters in AC Microgrids," in IEEE Transactions on Power Electronics, vol. 27, no. 11, pp. 4734-4749, Nov. 2012, doi: 10.1109/TPEL.2012.2199334.

[27] J. A. Pecas Lopes, C. L. Moreira and A. G. Madureira, "Defining control strategies for analysing microgrids islanded operation," 2005 IEEE Russia Power Tech, 2005, pp. 1-7, doi: 10.1109/PTC.2005.4524548.

[28] J. M. Guerrero, J. C. Vasquez, J. Matas, L. G. de Vicuna and M. Castilla, "Hierarchical Control of Droop-Controlled AC and DC Microgrids—A General Approach Toward Standardization," in IEEE Transactions on Industrial Electronics, vol. 58, no. 1, pp. 158-172, Jan. 2011, doi: 10.1109/TIE.2010.2066534.

[29] Phi-Long Nguyen, Q. Zhong, F. Blaabjerg and J. M. Guerrero, "Synchronverter-based operation of STATCOM to Mimic Synchronous Condensers," *2012 7th IEEE Conference on Industrial Electronics and Applications (ICIEA),* Singapore, 2012, pp. 942-947, doi: 10.1109/ICIEA.2012.6360859.

[30] G. Li, F. Ma, Y. Wang, M. Weng, Z. Chen and X. Li, "Design and Operation Analysis of Virtual Synchronous Compensator," in *IEEE Journal of Emerging and Selected Topics in Power Electronics*, vol. 8, no. 4, pp. 3835-3845, Dec. 2020, doi: 10.1109/JESTPE.2019.2943723.

[31] C. Li, R. Burgos, I. Cvetkovic, D. Boroyevich, L. Mili and P. Rodriguez, "Analysis and design of virtual synchronous machine based STATCOM controller," *2014 IEEE 15th Workshop on Control and Modeling for Power Electronics (COMPEL)*, Santander, 2014, pp. 1-6, doi: 10.1109/COMPEL.2014.6877134.

[32] D. Sera, L. Mathe, T. Kerekes, S. V. Spataru and R. Teodorescu, "On the Perturb-and-Observe and Incremental Conductance MPPT Methods for PV Systems," in IEEE Journal of Photovoltaics, vol. 3, no. 3, pp. 1070-1078, July 2013, doi: 10.1109/JPHOTOV.2013.2261118.

[33] Bala Subramanian, Sridhar, "State Space Modeling of Smart PV Inverter as STATCOM (PV-STATCOM) for Voltage Control in a Distribution System" (2016). *Electronic Thesis and Dissertation Repository*. 3764.